Throwing Manipulation: Design, Identification, and Learning-Based Control for a Novel Throwing End-Effector

Thesis submitted in partial fulfilment
of the requirements for the degree of

Master of Science in
Electronics and Communication Engineering
by Research

by

PASALA HAASITH VENKATA SAI
2021702017
HAASITH.PASALA@RESEARCH.IIIT.AC.IN

International Institute of Information Technology
Hyderabad - 500 032, INDIA
June 2024

International Institute of Information Technology
Hyderabad, India

CERTIFICATE

It is certified that the work contained in this thesis, titled "Throwing Manipulation: Design, Identification, and Learning-Based Control for a Novel Throwing End-Effector" by Pasala Haasith Venkata Sai, has been carried out under my supervision and is not submitted elsewhere for a degree.

Date

Adviser: Dr. Nagamanikandan Govindan

To My Family and Teachers

Acknowledgments

I am deeply grateful to my advisor, Dr. Nagamanikandan Govindan, for his unwavering support, guidance, and mentorship throughout the course of my thesis. His expertise, encouragement, and constructive feedback have been instrumental in shaping the trajectory of my research and honing my skills in the dynamic field of robotics.

I am especially thankful to my family for their unwavering support in all my endeavours, allowing me to explore my interests and flourish. Their love and encouragement are invaluable, and I am deeply grateful for their unwavering presence throughout my academic journey.

During my tenure at RRC, I've been fortunate to have the support and guidance of numerous colleagues who have helped me grasp and comprehend the intricacies of my field. I extend my heartfelt gratitude to Laksh, Aanjaney, Priyansh, Aravind, Damodar, Sanket, Prateek, Sumanth, Rishabh, Aditya, Bharadwaj, Sourav and all my fellow colleagues at RRC for their unwavering support and belief in my abilities. The Robotics Research Center (RRC) welcomed me with open arms, and I am deeply grateful for the inclusive environment it provided. I've been fortunate to have wonderful friends who consistently pushed me beyond my comfort zone and instilled in me a deep appreciation for research. To everyone at RRC, I extend my sincere thanks for your acceptance, inspiration, and unwavering motivation from the very beginning.

I would also like to extend my gratitude to Dr. Samarth Brahmbhatt, who has been instrumental in our recent work, particularly in matters related to machine learning. His expertise and contributions have significantly enriched the quality and scope of my research.

Lastly, I express my gratitude to the institute for providing a platform for aspiring researchers to pursue their dreams and develop themselves in the process. I am deeply appreciative of the support and resources made available to me throughout my academic journey. Additionally, I thank the thesis examiners for their valuable feedback, which played a crucial role in improving this thesis. Their insights and suggestions have been invaluable in refining the quality of my work.

Thank you all.

Abstract

With the advent of Industry 4.0, the demands on industrial robots have expanded beyond simple pick-and-place tasks. Future smart factories require robots capable of a wide range of manipulation skills, including the ability to throw objects. This thesis investigates the design and optimization of a novel robotic end-effector that manipulates objects by enabling precise grasping and target throwing.

Current robotic grippers primarily focus on grasping, while throwing is typically achieved through energy-intensive whole-arm movements. This approach is not only inefficient but also raises safety concerns. To address these limitations, this research proposes a versatile gripper that seamlessly integrates pick-and-place and pick-and-throw functionalities using stored elastic energy. The controlled release of this energy propels objects with accuracy, potentially exceeding the robot arm's reachable workspace.

Key contributions of this research include:

- **Novel End-Effector Design:** The design of a new end-effector capable of performing pick, place, and throw actions without relying on whole-arm motion. This innovative design leverages stored elastic energy for throwing, thus enhancing efficiency and safety.
- **Physics-Based Model:** A physics-based model that accurately correlates the stretch of an elastic band to the landing position of the thrown object. This model integrates the principles of rigid body dynamics to account for the object's behaviour during projectile motion, making it essential for predicting and controlling the trajectory of thrown objects.
- **Parameter Identification:** Implementation of a two-stage process to identify the parameters of the physics-based model. This process ensures that the model accurately reflects the behaviour of the end-effector.
- **Optimal Control Algorithms:** Development of sophisticated control algorithms that enable the robot to throw objects to specific target locations with high precision. These algorithms calculate the optimal release point and force required for each throw.

- **Data-Driven Residual Model:** Development of a data-driven residual model to capture unmodeled dynamics and further improve throwing accuracy. This model uses machine learning techniques to refine predictions based on experimental data.
- **Experimental Validation:** Conducting experiments to validate the effectiveness of the end-effector design and its control algorithms. These experiments demonstrate the practical viability and robustness of the proposed system.

The thesis further explores the vast practical implications of throw manipulation. In warehouse logistics, this technology can significantly optimize sorting, packing, and distribution processes by enabling faster and more precise handling of items. In agriculture, it holds the potential to be used for harvesting, seeding, and the targeted application of resources, leading to increased efficiency and reduced labour costs.

By combining optimization and learning-based approaches, this research provides a comprehensive framework for designing and optimizing robotic end-effectors for throwing manipulation. This interdisciplinary methodology enhances the versatility, adaptability, and performance of robots, ultimately improving efficiency, safety, and productivity in various industrial and operational settings.

Keywords: Throwing manipulation, Gripper design, Trajectory optimization, Rigid body dynamics, Learning-based approaches.

Contents

List of Figures

List of Tables

Chapter 1

Introduction

1.1 Background

As Industry 4.0 advances, manufacturing industries strive to enhance performance by optimizing production operations. Consequently, robots have evolved beyond simple pick-and-place tasks and limited workspaces, particularly in industrial and warehouse settings. While mobile bases, such as mobile manipulators (MM), provide the advantage of horizontal mobility, they often face limitations in vertical reach, making it challenging to access elevated shelves in multi-rack storage systems. Similarly, drones are increasingly utilized in warehouses for transporting objects; however, they encounter difficulties due to ground effects when the target location is partially enclosed or confined, which is frequently the case in multi-rack storage setups.

In such scenarios, there is a need for robots with targeted throwing capabilities to place objects beyond their limited reachable workspace. Research on object-throwing robots in industrial settings has attracted significant interest recently due to their ability to transport materials faster than conventional methods. For instance, rather than utilizing mobile manipulators or conveyor belts for inter-station object transport, integrating a specialized end-effector with either a moving or fixed base yields notable reductions in object transport time, mechanical exertion, and effort, resulting in enhanced efficiency and cost savings.

The task of sorting or segregating diverse objects on a moving conveyor belt often necessitates the involvement of multiple manipulators, leading to inherent limitations and operational challenges. In contrast, the implementation of throwing manipulation presents the opportunity to minimize the reliance on multiple robots. This method allows for a more streamlined operation where a single robotic system can handle multiple tasks, reducing the need for complex coordination and increasing overall efficiency.

Despite the demonstration of numerous simple robotic hands, a simple and standalone shape-conformable gripper capable of throwing is hard to find in the literature. In predominant works related to throwing tasks, manipulators are commonly employed to place the object outside the workspace. In many such situations, trajectory optimization techniques are used to actuate the joints in a coordinated way at high speed to gain increased momentum for throwing an object away from its limited workspace. Implementing such techniques requires computationally expensive planning and control algorithms at the cost of immense joint motor efforts. Furthermore, the mechanical components would easily be worn out because of rapid movements, reducing the overall system's performance.

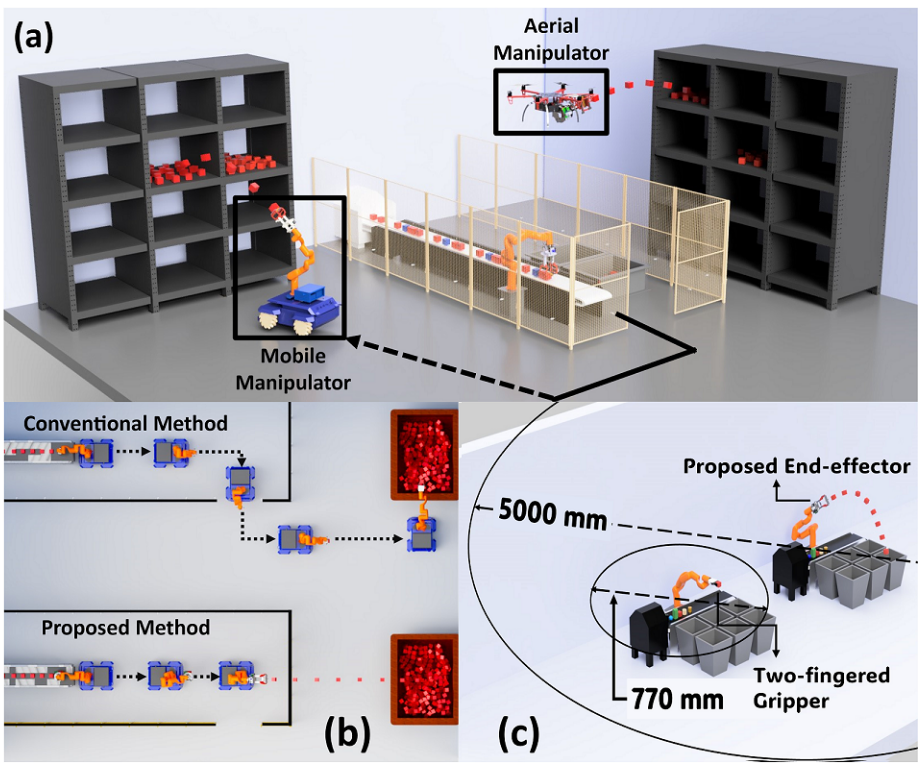

Figure 1.1: (a) illustrates the throwing end-effector using mobile and aerial manipulators in an industrial setting. (b) compares the conventional method with a gripper to the proposed method with the throwing end-effector, highlighting increased workspace and reduced energy consumption. (c) displays the reachable workspace of the manipulators with both methods.

1.2 Motivation

The motivation behind this research stems from the pressing need to enhance the operational efficiency and capabilities of robotic systems in various industrial applications. Traditional methods of object transport and manipulation, such as conveyor belts and mobile manipulators, often encounter limitations in speed, efficiency, and spatial reach. These constraints become particularly pronounced in environments with complex storage systems or confined spaces, such as multi-rack storage systems in warehouses or enclosed target locations for drones.

Inspired by biological agents that use elastic-based catapult or slingshot mechanisms for remarkable ballistic/projectile movements, this research aims to develop a novel gripper that mimics these natural mechanisms. Biological agents possess extraordinary multifunctional morphology that is superior, versatile, and quickly adapt to various situations. Many such agents use elastic-based mechanisms to store elastic strain in muscles, ligaments, tendons, or fibrous structures and use them for remarkable ballistic/projectile movements.

Examples include the jumping of frogs and click-beetles [1], ballistic tongue projection in chameleons and salamanders for prey capture [2], predation and propulsion in trap-jaw ants [3], and the dispersion of seeds among plants [4]. These mechanisms allow biological agents to achieve significant acceleration and precision in their movements, which are essential for survival and efficiency in their natural habitats. Throwing is also typical among humans [5] for handling and placing objects with incredible speed for quick rearrangement, sorting tasks, and traversing over large obstacles. This method is preferred for the increased economy of movement, particularly when the object needs to be placed outside the reachable workspace of an agent.

By leveraging these biological principles, the research seeks to develop a gripper that can store and release energy efficiently, similar to a catapult mechanism found in nature. The proposed gripper integrates advanced design principles, trajectory optimization techniques, and learning-based approaches to enhance its throwing capabilities. This allows the gripper to achieve high-speed, precise, and adaptable throwing actions, making it suitable for various industrial applications.

The primary motivation is to create a robotic system that can perform tasks beyond the limitations of current technologies, providing increased productivity, reduced operational costs, and improved outcomes. By addressing the challenges of object manipulation and transport in confined and complex environments, this research aims to advance robotic systems, paving the way for future innovations in the field.

A combination of contracting muscles equivalent to springs and a latching mechanism, i.e., a catapult mechanism, is common among many biological agents. They primarily use these mechanisms to amplify the limited mechanical power output to a greater extent. The elastic mechanism's quick unlatching enables them to instantly release the energy to achieve significant acceleration for capturing prey or using it as a defensive mechanism. The latching mechanism found in biological agents is discussed in [6, 7]; however, utilizing it for throwing is hard to find in the literature.

Many biological agents have inspired researchers to develop multipurpose mechanisms, particularly robotic hands, to perform dexterous tasks. Generally, shape conformation for versatile grasping, primitive manipulation for changing the object state, and contact force adjustment for robustness are the significant functionalities expected from robotic hands [8, 9]. However, demanding multiple functionalities inevitably increases actuators and sensors and, consecutively, the design's complexity. As pointed out in [10,11], the tradeoff between versatility and simplicity is evident in many existing gripper designs. Despite the demonstration of numerous simple hands earlier, a simple and standalone shape conformable gripper capable of throwing is hard to find in the literature. In predominant works related to throwing tasks [8, 9], manipulators are commonly employed to place the object outside the workspace. In many such situations, trajectory optimization techniques are used to actuate the joints in a coordinated way at high speed to gain increased momentum for throwing an object away from its limited workspace. Implementing such techniques requires computationally expensive planning and control algorithms at the cost of immense joint motor efforts. Furthermore, the mechanical components would easily be worn out because rapid movements reduce the overall system's performance.

The design integrates elastic and rigid elements with a central latching mechanism that controls the storage and release of elastic potential energy. The latching mechanism mechanically actuates two rigid fingers by elongating and releasing the coupled elastic gripping surface, akin to soft tissues in biological agents, as illustrated in Fig. 2.4. During grasping, the rope attached to the elastic strip is pulled inward by the latching mechanism, increasing tension and storing elastic potential energy. Figures 2.4 (a)-2.4 (c) depict the mechanical actuation and grasping sequence, while Figure 2.4 (d) shows the elastic surface conforming to objects of various shapes, sizes, and weights.

For placing tasks, the mechanism must gradually release the stored energy to avoid imparting kinetic energy to the object, preventing bounce or topple. Conversely, for throwing tasks, the mechanism must instantly release the energy to propel the object, enabling it to reach beyond the robot's immediate workspace. The amount of elastic energy released can be predetermined for precise control.

1.3 Research Objectives

The research objectives of this thesis entail a comprehensive approach to developing an end effector and integrating it with manipulators and drones to enhance their functionality in industrial settings. The objective involves designing and fabricating an innovative end effector capable of performing dynamic manipulation tasks. This entails conceptualizing a versatile gripping mechanism that can adapt to various object shapes and sizes, ensuring robust and efficient handling capabilities. Integration with manipulators and drones will enable seamless interaction with the surrounding environment, facilitating tasks such as pick-and-place operations, object transport, and assembly tasks.

Secondly, the research aims to define the rigid body dynamics governing objects in projectile motion. This involves a detailed analysis of factors such as mass distribution, inertia, and aerodynamics to accurately model the behaviour of objects during throwing manipulation. System identification techniques will extract relevant parameters from experimental data, ensuring the model's fidelity in representing real-world scenarios.

Furthermore, the thesis seeks to develop a data-driven model integrated with an optimal control algorithm to optimize the trajectory of thrown objects. By leveraging machine learning and optimization techniques, the aim is to achieve precise control over the motion of objects. This involves formulating and solving optimal control problems tailored to the specific dynamics of the system, considering constraints such as actuator limitations, physical limitations of the prototype and environmental factors.

The study explores practical applications, showcasing throwing manipulation's versatility in warehouse logistics, agricultural operations, and search and rescue scenarios. In warehouses, it facilitates efficient sorting, packing, and distribution, optimizing space utilization and streamlining processes. In agriculture, it aids fruit harvesting, crop seeding, and targeted application of pesticides or fertilizers, enhancing productivity while minimizing waste. In search and rescue, it enables rapid deployment of equipment and resources to remote or hazardous locations, augmenting rescue team capabilities.

Finally, the research involves performing experiments with hardware implementation to validate the effectiveness and efficiency of the developed end effector and control algorithms in real-world scenarios. The research aims to demonstrate the proposed approach's feasibility and efficacy in enhancing robotic systems' capabilities for industrial automation and logistics tasks through systematic experimentation and validation.

1.4 Related Works

The field of throwing manipulation has garnered significant attention in recent years due to its potential to enhance the efficiency and capabilities of robotic systems in various industrial and operational contexts. This section reviews the existing literature on throwing manipulation, nonprehensile manipulation, and gripper design, highlighting the advancements and challenges in these areas.

Several studies discuss throwing as a form of non-prehensile manipulation, utilizing either single-joint or multi-joint robot arms. Typically, these manipulators impart the initial velocity and acceleration to the object while maintaining contact and subsequently release the object to take flight towards the desired location [12–14]. This process is generally formulated as a motion planning problem, wherein the manipulator's trajectory is optimized to deliver the object accurately [15, 16]. Some researchers have applied learning approaches or optimal control techniques to improve the throwing capabilities of manipulators. However, the complexity of the planning and control algorithms, increased effort, and scalability issues remain significant challenges.

Most existing works employ manipulators with standard grippers to grasp and throw objects by actuating all joint motors and releasing the object at an optimal release point [17]. This method often requires computationally expensive algorithms and higher energy consumption. For example, TossingBot utilizes a manipulator to grasp objects from an unstructured bin and throws them into a target box, but this requires high-speed actuation of all joints, leading to concerns about wear and tear, safety, and power consumption [17]. Reinforcement learning approaches have also been explored for learning whole-arm throwing motions [5].

Nonprehensile grasping methods have been investigated to enhance the efficiency of throwing tasks. For instance, a casting manipulator with a flexible string attached to a gripper extends the manipulator's workspace [18]. Additionally, nonprehensile methods such as stone-throwing mobile robots for curling [19] and conveyor belt-fed single-joint arms [20] have been explored. However, these methods often lack prehensile capabilities, limiting their versatility and application scope.

Numerous studies have focused on replicating the capabilities of anthropomorphic hands to achieve different types of grasp and within-hand manipulation [21, 22]. Due to the design complexities and challenges associated with complex hands, minimalistic robotic hand designs have gained attention. These designs aim to provide mechanical intelligence, improve dexterity, and simplify mechanical complexity. Many adaptive grippers, such as soft grippers [23,24], origami grippers [25], underactuated grippers [26–28], and compliant grippers [29,30], exhibit exceptional power grasp ability essential for stable and robust grasping. Some grippers incorporate variable friction finger pads [31] to enhance dexterity, albeit at the cost of additional motors and increased complexity. A notable example is a vacuum-based universal robotic gripper [32], capable of picking, placing, and limited-distance throwing of objects. Nonetheless, many grippers still struggle with grasping and throwing objects independently.

Similarly, [33] and [34] demonstrate the whole-arm motion for throwing learned with reinforcement learning. A soft gripper based on vacuum technology is showcased in [32], capable of picking and placing objects and limited-distance throwing. This approach has inherent drawbacks, including limited repeatability, reduced precision, and lower grasping force. Deep reinforcement learning approaches for learning whole-arm throwing motion are shown in [35] and [36] while avoiding obstacles and for a soft-bodied robot, respectively.

To address the limitations of existing grippers, hybrid designs combining soft and rigid elements have been proposed. The proposed design aims to retain the shape-conforming capabilities of soft hands while enhancing mechanical robustness and simplifying the overall structure. The hybrid design integrates the advantages of both soft and rigid elements [37], actuated mechanically using a latch mechanism without a pneumatic source. This approach ensures compactness, simplicity, and energy efficiency while maintaining the functionality of soft hands. As a part of this research, two end-effector designs were proposed, i.e., Design 1.0 and Design 2.0. Design 2.0 has improved controllability, effectiveness, and independent actuation for regulating the energy stored for throwing objects. This enhanced 2 DoF end-effector is an advancement upon the prior design 1.0 [37], which suffered from limitations in adjusting stored elastic energy after grasping an object. Unlike the previous design, where stored energy could only be monotonically increased, the current design allows for regulation, enabling both increased and decreased stored energy as required. Additionally, the mechanical design is significantly simplified, with fewer moving parts.

1.5 Overview of the Thesis structure

The thesis is organized into six chapters, each offering a detailed exploration of different aspects of throwing manipulation in robotics. Below is a summary of each chapter:

- **Chapter 1: Literature Review** This chapter comprehensively explores relevant literature on throwing manipulation, end-effector design, mathematical modelling, system identification, throw optimization, and learning-based approaches. It synthesizes prior research findings, offering valuable insights while identifying gaps and addressing current challenges. This review lays the groundwork for developing novel solutions and methodologies in subsequent chapters.

- **Chapter 2: Design of Throwing Mechanism** This chapter focuses on the novel end-effector designs 1.0 and 2.0. for throwing manipulation. It covers the functional requirements, material selection, and mechanical design principles for developing the gripper and its components. Detailed discussions include the actuation system, force transmission components, control systems, and their integration with the robot's overall architecture.

- **Chapter 3: Mathematical Modeling** This chapter delves into the mathematical modelling of the gripper and the dynamics of an object in projectile motion, building on the foundations laid in Chapter 2. It provides a comprehensive theoretical framework for the optimization and control strategies discussed in Chapter 4.

- **Chapter 4: Optimization and Parameter Identification** This chapter focuses on optimization and parameter identification to achieve optimal throwing performance. It derives equations of motion and identifies physical properties through sensor data analysis and experiments to calibrate the mathematical models using a two-stage optimization algorithm. The chapter also discusses the Throw optimization algorithm to generate optimal throwing trajectories, considering environmental factors and object properties.

- **Chapter 5: Integration of Machine Learning Algorithms** This chapter explores the integration of machine learning algorithms to enhance the adaptability and performance of throwing manipulation tasks. It presents the theoretical foundations, implementation details, and experimental results demonstrating the effectiveness of learning-based approaches in improving system performance with unseen objects.

- **Chapter 6: Discussion and Conclusion** The final chapter presents research findings, offering insights and interpretations, acknowledging limitations, and outlining avenues for future research. It highlights the study's significance and implications for throwing manipulation and robotics. By integrating theoretical analyses, experimental results, and practical considerations, this chapter provides a cohesive conclusion to the thesis and paves the way for future innovations in the domain.

These chapters offer in-depth analyses of theoretical foundations, implementation details, experimental results, and discussions of findings.

Chapter 2

End-Effector Design and Working Principle

The end-effector mechanism draws inspiration from the efficiency and simplicity of a slingshot. Like the traditional handheld tool, this mechanism utilizes elastic energy stored in a tensioned element to propel objects with precision and speed. By harnessing this principle, the end-effector achieves dynamic manipulation capabilities crucial for industrial tasks such as pick-and-place operations and targeted throws.

At its core, the mechanism consists of a tensioning system, akin to pulling back the elastic band of a slingshot, and a release mechanism to propel the object towards its intended target. This design ensures efficient energy transfer and precise control over object trajectories. Furthermore, the mechanism's simplicity facilitates ease of maintenance and operational reliability, essential for seamless integration into industrial environments.

In this section, we delve into the intricacies of the slingshot-inspired mechanism, detailing its components, functionality, and advantages in achieving versatile and efficient robotic manipulation. We'll also compare the two versions of the end-effector, highlighting the improvements made in the current streamlined design.

2.1 Design Version 1.0

2.1.1 Gripper Mechanism

The embodiment of the proposed end-effector design 1.0 [37] is shown in Fig. 2.1(a). The gripper consists of two rigid fingers (F1 and F2) pivoted at the base plate and preloaded with torsional springs (TS1 and TS2) to enable passive actuation. The fingers have angle limiters fitted to the base plate, controlling the maximum opening and closing angles. The rigid finger geometry is designed to maximize the within-hand workspace, accommodating objects when the fingers are fully closed, similar to the methodology discussed in [38]. An elastic strip routes from the rear side of one finger (F1) to the central hoop and ends at the backside of the other finger (F2). The central hoop connects to the latching mechanism (LM) via ropes. Passive rollers (P1 and P2) are provided at each finger's end to reduce traction between the elastic strip and rigid elements with parallel axes. The elastic element's advantage is that the motor power density does not limit the object's take-off velocity, resulting in an initial velocity much larger than achievable by the driving motor's speed.

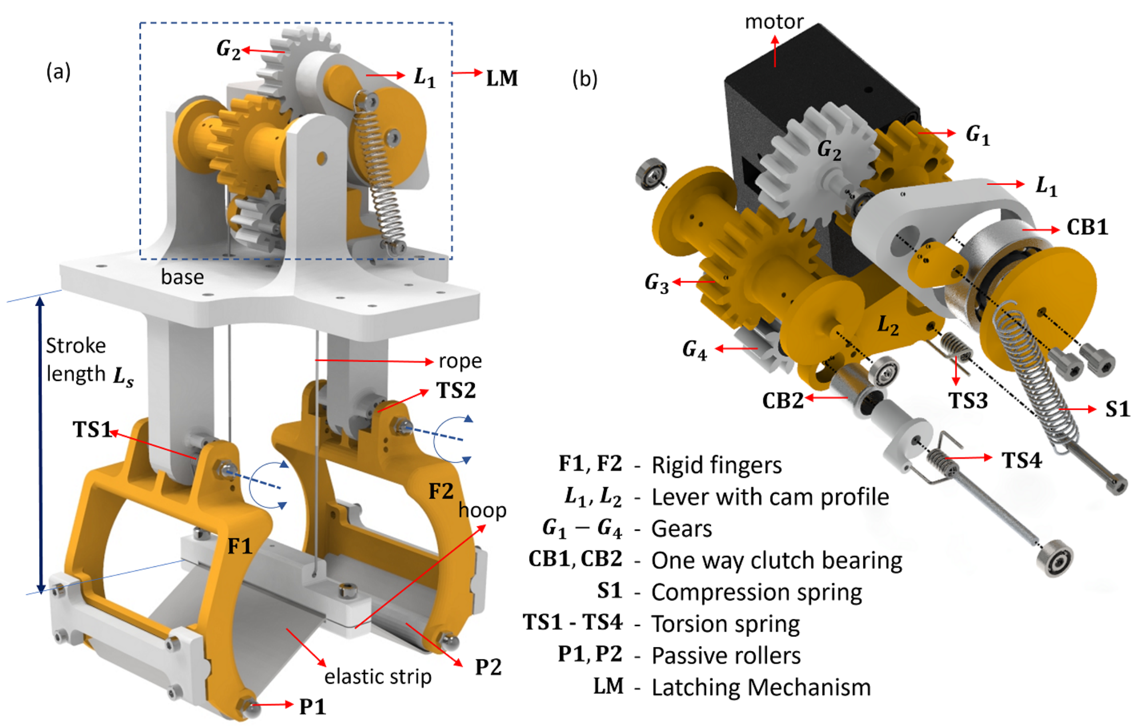

Figure 2.1: Design of the multi purpose gripper.(a)Rendered computer-aided design(CAD) model of the gripper mechanism.(b)Exploded view of the LM.

2.1.2 Latching Mechanism Design

Figure 2.1(b) shows the latching mechanism, acting as the driving unit and playing a crucial role in switching between throwing and placing tasks. A switching mechanism without additional actuators is critical, as energy must be instantly released for throwing an object and slowly released for impact-free placing. The latching assembly consists of a drive motor (XM540 Dynamixel^{TM}), two cam-based spring-loaded lever subassemblies, and a spool drum. The first lever assembly comprises a sun gear (G_1), planetary gear (G_2), a spring-loaded arm with a cam profile (L_1), and a one-way clutch bearing (CB1). The gear G_2 revolves around G_1, and they are held together by the movable arm L_1. The gear G_1 is rigidly attached to the motor horns, and the spool drum is attached with a third gear (G_3) for winding the rope. The bearing CB1's inner and outer races are rigidly connected to G_1 and the spring-loaded arm L_1, respectively. Since CB1 transfers torque in the clockwise direction (CW) and moves freely in the counterclockwise direction (CCW), the arm L_1 must be spring-loaded (S1) to ensure contact between G_2 and L_1. Doing so transfers the motor's CCW motion from G_1 to G_2 via L_1. The drum attached to G_3 can rotate about its axis and provided with flanges on both ends to prevent the rope from derailing during latching or unlatching.

The second lever assembly serves as a torque reducer. It comprises G_4, a torsion spring (TS3) loaded arm with a cam profile (L_2), and a gear G5 whose axis coincides with a one-way clutch bearing (CB2) and torsion spring (TS4). In this arrangement, the torsion spring (TS4) is attached between the inner race of CB2 and the arm L_2. The outer race of CB2 is rigidly connected to G5. The torsion spring (TS3) at the pivot of L_2 keeps L_2 and G_4 in contact. This subassembly is called a torque reducer. The torque reducer is designed to produce reaction torque at L_2 in CCW to restrict the CW motion of G_4. The functionality of CB2 is crucial to hold the rope tension while holding an object and permit L_2 to rotate while winding up the rope.

2.1.3 Working Principle

In the previous section, the design details of the gripper were presented. This section discusses the working principle of a single actuator-based latching mechanism for grasping, impact-free placing and throwing of an object. Figures 2.2(a) to 2.2(d) illustrate the schematic and operating sequence of the proposed latching mechanism. Figure 2.3 depicts energy transfer at different stages of latching and unlatching.

2.1.3.1 Grasping

Due to the one-way clutch bearing (CB1) and the mechanical arrangement of the lever assembly (the spring-loaded L_1 keeps G_2 in contact with G_3), rotating the motor in the clockwise (CW) direction removes the contact between G_2 and G_3. At rest, G_2 maintains contact with G_3 due to the counterclockwise (CCW) moment generated by the spring-loaded arm (L_1), as shown in Fig. 2.2(a). By rotating the motor in the CCW direction, the motion is transferred to G_3, which in turn rotates the spool drum in the CCW direction and winds the rope, as de-

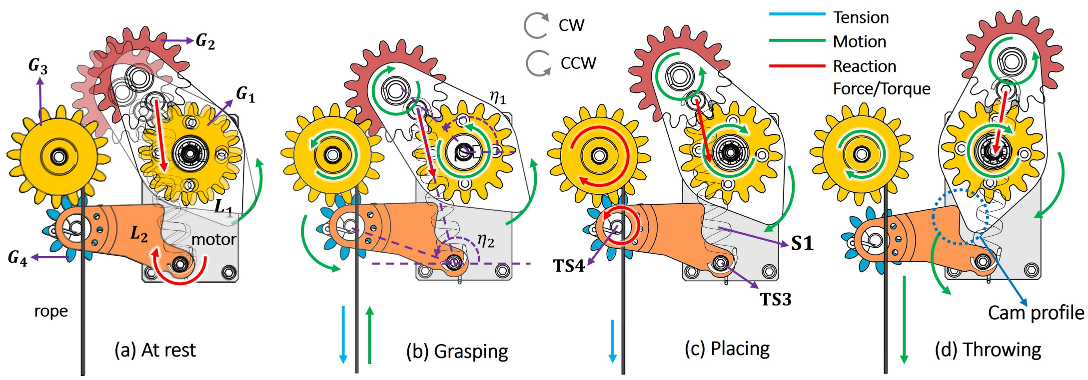

Figure 2.2: Stages of operation of latching mechanism: (a) At rest (b) Grasping (c) Placing (d) Throwing.

picted in Fig. 2.2(b). The gears transfer the applied motor torque to G_3 through tooth contacts. Considering ω_1 as the motor speed, the speed of the spool attached to G_3 is:

$$\omega_3 = \frac{N_2}{N_3}\frac{N_1}{N_2}\omega_1 \tag{2.1}$$

Where ω_i and N_i are the angular velocity and number of teeth of the gear G_i, respectively. Assuming a no-slip condition, neglecting all frictional losses, and taking the gear reduction ratios as one, the transmitted power remains unchanged during the grasping phase.

$$\tau_{G_1}\omega_1 = \tau_{G_2}\omega_2 = \tau_{G_3}\omega_3 \tag{2.2}$$

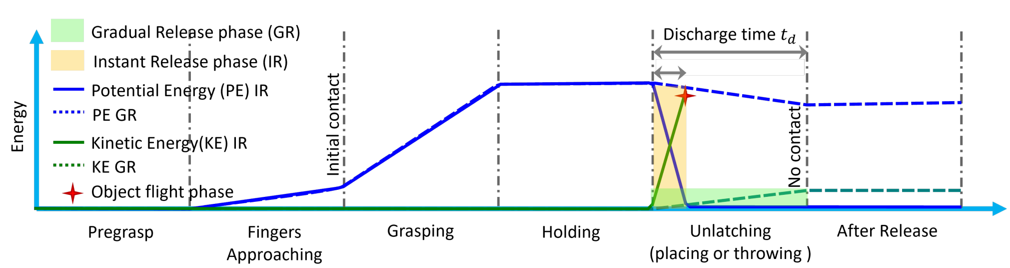

Figure 2.3: Energy diagram showing the levels of energy stored and discharged at various stages of operation.

This phase is called the grasping phase since the motion of G_3 rotates the spool drum, which in turn winds the rope attached to the elastic element through a hoop, as observed in

Fig. 2.4(a)-(c). Consecutively, the potential energy of the elastic surface ($V_{elastic}$) increases gradually along with the closure of the spring-loaded rigid fingers about its pivot axis until the limited maximum closure angle (refer to the grasping phase in Fig. 2.3). When the object is held only due to soft contact (Fig. 2.4(d)) or no contact (Fig. 2.4(a)), then the total stored energy V_{total} is:

$$V_{total} = V_{elastic} + V_{spring} \tag{2.3}$$

Where $V_{spring} = \frac{1}{2}K_s\theta_s^2$ is the potential energy of the torsion spring, K_s and θ_s are the stiffness and angular displacement of the spring (TS_1 and TS_2), respectively. The potential energy stored in the elastic strip $V_{elastic}$ has been experimentally determined, as discussed in Section V. Although G_3 is in contact with G_4, due to CB_2, the CW moment τ_{G_4} is zero. As a result, G_4 rotates freely in the CW direction at the speed of:

$$\omega_4 = \frac{N3}{N4}\omega_3 \tag{2.4}$$

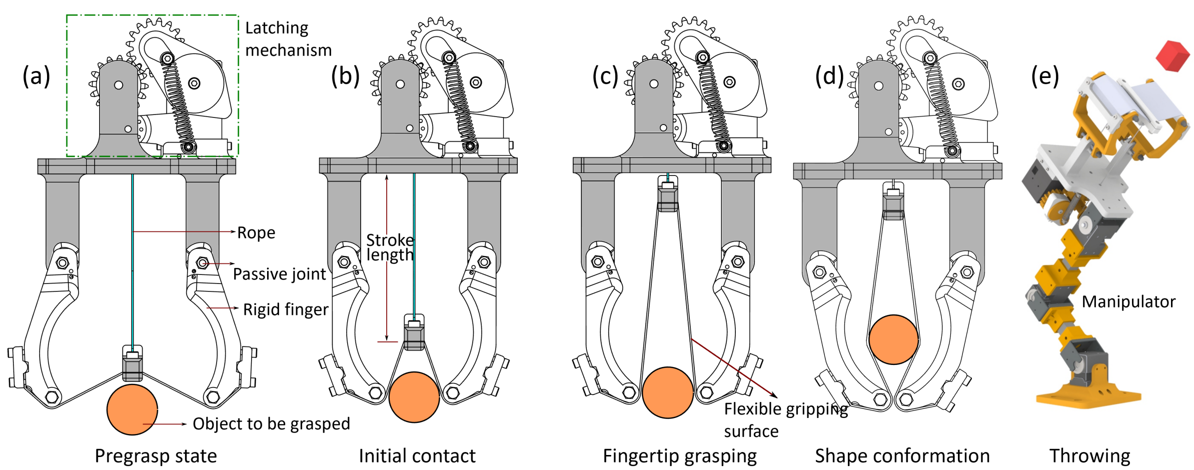

Figure 2.4: Schematic of the proposed gripper and its various phases of operation: (a) Pregrasp state (b) Initial contact (c) Fingertip grasping (d) Shape conformation (e) Throwing.

As the rigid fingers start to move inward (refer to Figures 2.4(a) and 2.4(b)), the elastic element establishes initial contact on an object. The gripping forces at the object increase as the elastic strain increases (refer to Fig. 2.4(c) and Fig. 2.3, grasping phase) by rotating the drum in the CCW direction or reducing the stroke length L_s (relative distance between the base plate and rigid hoop, as shown in Fig. 2.1 further. Using (2.2), the torque experienced by the motor due to the rope tension T is calculated from the following equation:

$$\tau_{G_1} = -r_{drum}T \tag{2.5}$$

Where r_{drum} is the spool drum radius.

2.1.3.2 Impact-free Placing – Gradual Release of Energy

After grasping the object, the stored elastic energy is retained as long as G_2 remains in contact with G_3. The contact must be removed by moving the arm L_1 to release the object, as illustrated in Fig. 2.2(c). At this stage, the subsequent free-rolling of G_3 must be restricted to ensure the impact-free placing of an object. Otherwise, the stored elastic potential discharges instantaneously, and the object gains acceleration and collides with the environment.

As the lever L_1 is rotated in the CW direction, and if no other external forces are acting on G_3, then the rope tension T due to the restoring elastic potential rolls the drum G_3 in the CW direction. However, due to the torsion spring TS4 with a stiffness K_4 of G_4 being in contact with G_3, the torque of G_3 deflects the spring (TS4) on G_4, which in turn resists the rotation of G_3. This is because one end of the spring TS4 is connected to G_4, and the other is mounted to the one-way clutch bearing, which locks the motion of G_4 in the CCW direction. The gear G_3 acts as a torque source, and G_4 has a respective restoring torque to counter the G_3 motion and the torque at the G_3 axis. This torque reduction is required to place the object without creating any collision or impact.

If the stiffness of TS4 at G_4 is stronger, then the contact cannot be broken, and the gripper still maintains the grasp. Therefore, the TS4 spring parameters are chosen to create a relatively less imbalanced torque between G_3 and G_4, sufficient to break the grasping contact (between the object and the gripper) instead of maintaining the torque equilibrium, as discussed below. Due to the unbalanced torques, G_4 experiences an angular acceleration. Consequently, G_4 deflects, and its spring potential increases and eventually (G_3 and G_4) reaches the torque equilibrium over time. The object loses contact with the gripper without gaining acceleration during the process, which is essential for placing the object without transferring the impact.

Dynamic Interaction between G_3 and G_4: Assume no friction at G_3 (i.e., damping coefficient, $B_3 = 0$), then the torque experienced by G_3 due to T is $\tau_{drum} = r_{drum}T$. Then, the gear contact force $f_c = \frac{\tau_{drum}}{r_3}$ between G_3 and G_4 must be equal and opposite (where r_i is the pitch circle radius of gear G_i). The following equations govern the dynamic interaction between G_3 and G_4:

$$f_c r_3 - I_3\omega_3 = 0 \tag{2.6}$$

$$f_c r_4 - I_4\omega_4 - B_4\omega_4 - K_4\theta_4 = 0 \tag{2.7}$$

Where θ_i, I_i, B_i, and ω_i are the angular position, moment of inertia, damping coefficient, and angular acceleration of the gear G_i, respectively. Using the arc length relation and defining θ_4 in the opposite direction of θ_3, we get $r_3\theta_3 = -r_4\theta_4$. Substituting it in (6) and (7) and simplifying them yields the equation of motion describing the natural dynamics of G_4:

$$\left(I_3\left(\frac{r4}{r3}\right)^2 + I_4\right)\omega_4 + B_4\omega_4 + K_4\theta_4 = 0 \tag{2.8}$$

The system parameters are intentionally chosen to achieve the characteristics of an over-damped system (damping ratio, $\zeta > 1$) by selecting $B_4 >> \sqrt{K_4\left(I_3\frac{r4}{r3}\right)^2 + I_4}$, so that G_3 and G_4 move slowly toward the torque equilibrium. Considering the roots of the equation with a smaller real part magnitude that dominates the time response, the time constant $t_d = \frac{1}{\zeta - \sqrt{(\zeta^2-1)}\omega_n}$ was found. The damping ratio and natural frequency are $\zeta = \frac{B_4}{2\sqrt{K_4\left(I_3\frac{r4}{r3}\right)^2 + I_4)}}$ and $\omega_n = \sqrt{\frac{K4}{\left(I_3\frac{r4}{r3}\right)^2 + I_4)}}$, respectively. If $t_d > 0$, the system response will eventually decay exponentially from the initial conditions towards zero, and the system remains stable, as can be inferred from Fig. 2.3 (refer to the gradual release phase during unlatching). Therefore, even a short discharge time t_d would be sufficient to break the grasping contact and nullify the acceleration gained by the grasped object due to stored elastic potential.

2.1.3.3 Throwing – Instant Release of Energy

The gripper must instantly discharge the stored elastic potential to propel the object outside the robot's reachable range. By stretching the elastic strip with a strain ϵ, the strip elongates to a length $(\epsilon + 1)L_0$, where L_0 is the free length of the elastic strip. In the proposed design, actively decreasing the stroke length L_s increases the elongation of the elastic strip, which is in contact with the grasped object. As the strain increases, the normal forces f_g at the contact area (between the elastic strip and the grasped object) and the elongated final length (L) also progressively increase since the strip is clamped at the object-gripper contact location, and the hoop end is moving. More elongation stores more elastic potential energy along the axial direction. Simultaneous release of the stored elastic energy and breaking of the grasp contact points facilitate the object to gain rapid acceleration and reach a far distance.

As the motor rotates in the CW direction (refer to Fig. 2.2(d)), due to the one-way clutch bearing and the other mechanical arrangements, L_1 overcomes the torque due to spring S_1 and rotates CW. As soon as the two eccentric cam profiles make contact (refer to Fig. 2.2(d)), the CW motion of L_1 pushes L_2 in the CCW direction; consequently, G_4 disengages from G_3. The immediate disengagement is crucial, achieved by rotating L_1 at a rated angular velocity.

Thereby, G_4 abruptly loses contact with G_3 connected to the spool drum that is passively pivoted about its axis. As a result, the parameters of G_4 vanish immediately, and the response of G_3 is solely based on equation (2.6):

$$\omega_3 = \frac{f_c r_3}{I_3} \tag{2.9}$$

The instantaneous angular acceleration of G_3 is ω_3, which aids the elastic element to gain linear acceleration and move towards the clamped end. Thereby, the object breaks contact with the gripper and immediately gains the initial rapid energy from the stored elastic potential. As the object enters the flight phase and accelerates in free space, the energy would be gradually dissipated due to aerial drag and collision with the environment. The strip is relaxed after releasing the stored potential energy, and the aversion of the elastic strip is avoided by the hoop tied with a rope. The reason for not using springs in place of elastic strips is that using springs may potentially yield and fail under high strain, reducing the object's kinetic energy.

2.2 Design Version 2.0

The upgraded design version 2.0 of the gripper incorporates several modifications to enhance its functionality and versatility. Building upon the previous version, this design aims to provide greater control, flexibility, and precision in regulating the stored elastic energy, enabling seamless transitions between pick-and-place and pick-and-throw operations.

2.2.1 Latching Mechanism Enhancements

2.2.1.1 Addition of a Second Motor (M_2)

A significant improvement in version 2.0 is the introduction of a second servo motor (M_2) to the latching mechanism. This addition allows independent control over winding and unwinding the thread or elastic element, providing better regulation and fine-tuning of the stored elastic energy.

2.2.1.2 Redesigned Latching Mechanism

The latching mechanism has been redesigned to incorporate the second motor (M_2). Motor M_1 is responsible for engaging and disengaging the contact between gears G_1 (attached to M_2)

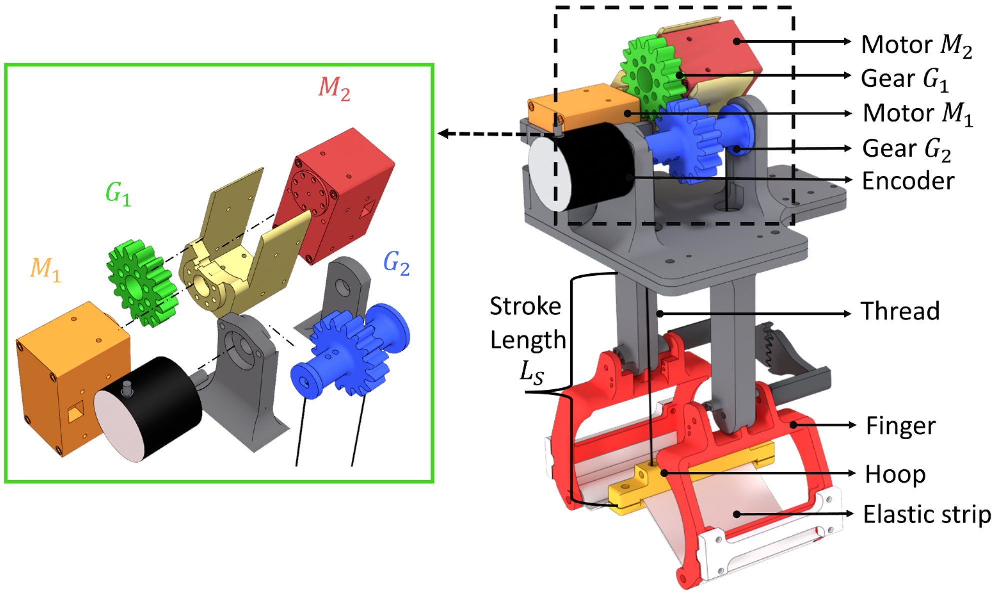

Figure 2.5: The CAD model of the EE with the proposed LM Design 2.0

and G_2 (connected to the spool drum). This redesign enables switching between pick-and-place and pick-and-throw modes efficiently.

2.2.1.3 Stroke Length Adjustment

Adding M_2 allows for precise stroke length adjustment (L_s), which is the effective length of the wound thread or elastic element. By winding or unwinding the thread using M_2, the stroke length can be set accurately, providing flexibility in controlling the amount of stored elastic potential energy.

2.2.1.4 Sensor Integration

An encoder is integrated with the spool drum to measure and estimate the stroke length (L_s). This sensor feedback enables accurate monitoring and control of the stored elastic potential energy, which is crucial for precise object manipulation.

2.2.1.5 Unwinding Capability

The previous version of the latching mechanism could only wind the thread in one direction. The new design, incorporating the second motor (M_2), allows for both winding and unwinding the thread. This capability is beneficial for adjusting the stroke length and preventing over-winding, thereby providing greater flexibility in energy management.

2.2.1.6 Gradual Object Release for Placing

The introduction of M_2 facilitates the gradual unwinding of the thread, enabling a controlled release of the stored elastic potential energy. This feature allows for the impact-free placing of objects by preventing the conversion of potential energy into kinetic energy, ensuring the object does not gain unwanted acceleration or initiate flight during placement.

2.2.1.7 Integration and Control

The end-effector version 2.0 is integrated with a Raspberry Pi 4 and a low-level controller for seamless operation. The controller manages the two servo motors (M_1 and M_2), enabling precise control over the latching mechanism and energy storage regulation. Additionally, it facilitates the measurement of the stroke length from the rotary encoder, providing essential feedback for accurate object manipulation.

With these enhancements, the gripper version 2.0 offers improved versatility, precision, and control in performing both pick-and-place and pick-and-throw tasks. The redesigned latching mechanism, coupled with the additional motor and sensor integration, enables fine-tuning of the stored elastic energy, ensuring smooth transitions between operational modes and optimal object manipulation.

2.2.2 Working Principle

This subsection details the working principle of the end-effector (EE) leveraging two motors for grasping, placing, and targeted throwing of objects.

2.2.2.1 Grasping:

Rotating M_1 in the clockwise (CW) direction rotates the lever attached to M_2 in the same direction, establishing contact between gears G_1 and G_2. With a gear ratio of one, powering M_2 in the counterclockwise (CCW) direction rotates G_1, which in turn induces a CW rotation in G_2. This motion extends to the spool connected to G_2, causing the thread to wind, as visually depicted in Fig. 2.6(i)-(ii). Consequently, the elastic element starts to move as it is tied up with the thread, and the elastic potential gradually increases. Concurrently, the pivoted fingers move inwards and successfully grasp the object.

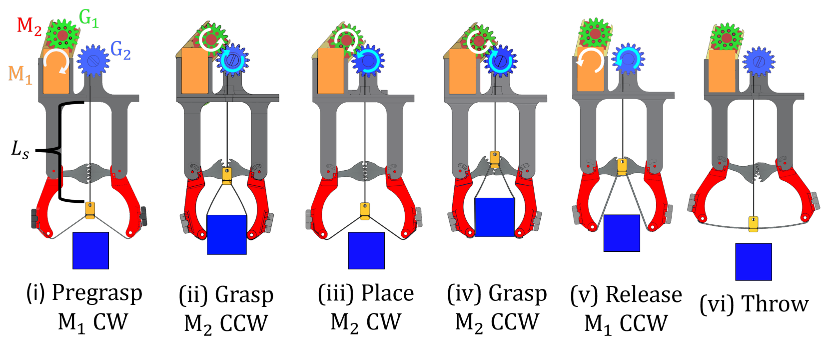

Figure 2.6: Illustrates the operational principles of the two DoF throwing EE. The action sequences for pick-and-place and pick-and-throw operations are shown in (i)-(iii) and (iv)-(vi), respectively, where M_i CW/CCW denotes the ClockWise/CounterClockWise rotation of the ith motor, G_i represents a gear, and arrows indicate the corresponding direction of rotation.

2.2.2.2 Placing:

The grasp remains secure as long as G_1 and G_2 are in contact. A CW rotation of M_2 gradually releases the stored elastic potential to facilitate impact-free placing. As a result, G_2 rotates in the CCW direction, unwinds the thread, and subsequently releases the object, as depicted in Fig. 2.6(iii). The gradual release ensures the placing of the object without gaining acceleration. This deliberate modulation prevents the conversion of stored potential energy into kinetic energy, effectively preventing the object from initiating flight motion.

2.2.2.3 Targeted Throwing:

When the task demands the throwing of an object to a distant location outside the robot's reachable range, the EE must rapidly discharge the stored elastic potential. This is achieved through a CCW rotation of M_1. Consequently, the instantaneous disengagement between gears G_1 and G_2 results in the immediate release of the thread, as illustrated in Fig. 2.6(v)-(vi). Simultaneously, the object gains kinetic energy, loses contact with the EE, and takes a flight motion to reach the desired distant location. The magnitude of the stored elastic potential is determined by measuring the stroke length (L_s).

The current chapter details an end-effector mechanism designed for industrial pick-and-place operations and targeted throws, inspired by a slingshot. The initial design (Version 1.0) features a gripper mechanism with torsional springs and an elastic strip for energy storage,

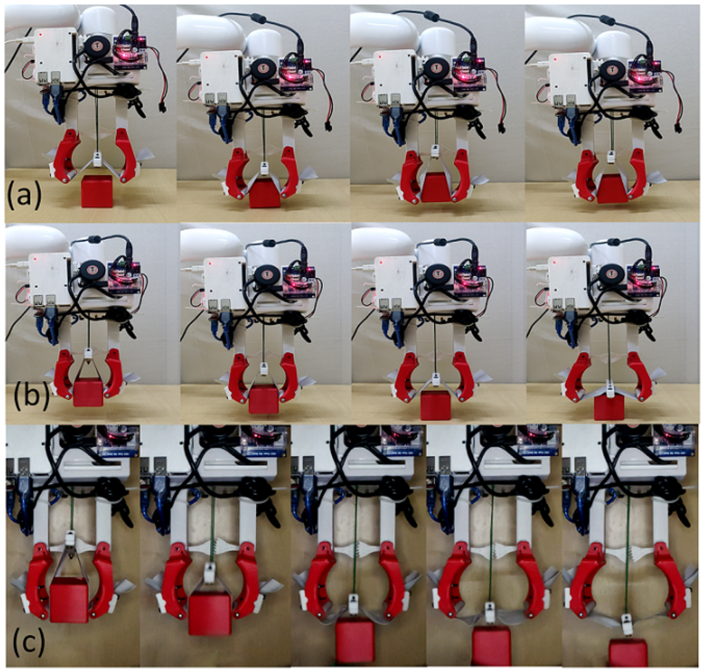

Figure 2.7: Illustrations of the working principle for grasping, placing, and targeted throwing: (a) Grasping, (b) Placing, (c) Targeted Throwing.

and a latching mechanism using a motor and cam-based levers for precise control of object placement and throwing. The improved Version 2.0 introduces a second motor for independent winding and unwinding, adjustable stroke length, sensor integration for accuracy, and enhanced control over energy release. This version offers more precision and versatility, ensuring efficient and gentle object handling. The next chapter will discuss the mathematical modelling and prototyping of the end effector, providing a deeper understanding of its design and functionality.

Chapter 3

System Modelling and Prototyping

This chapter details the modeling and prototyping of a versatile end-effector for industrial applications, inspired by biological mechanisms. The gripper combines elastic and rigid elements, utilizing a latching mechanism to store and release elastic potential energy for tasks such as shape-conformable grasping, impact-free placing, and controlled throwing.

We start by exploring the force-displacement relationship of the elastic strip through experimental setups, revealing its linear behaviour within a specific range. The mathematical relations are then developed to compute changes in the elastic strip's length during object grasping, enabling both power and fingertip grasps.

The chapter also covers the dynamics of the throwing system, including the parametric modeling of force impulse and object trajectory. Gripping force manipulation is validated experimentally and modelled to ensure reliable performance.

The prototyping section highlights the design and fabrication of the end-effector, emphasizing material selection and control mechanisms. Natural latex rubber strips were identified as the most effective for the gripper's needs. A laboratory prototype was developed and tested, demonstrating robust and versatile grasping capabilities.

3.1 Gripper Model

3.1.1 Elastic Strip's Force and Displacement Relationship

An experimental setup, as shown in Fig.3.1(a), is developed to determine the relationship between the axial force and elongation of the elastic strip. The force gauge is placed on an axially movable platform to measure the elastic force (f_{et}) exerted by the elastic strip under elongation. Preliminary experiments were conducted using the TheraBand Silver (Thickness

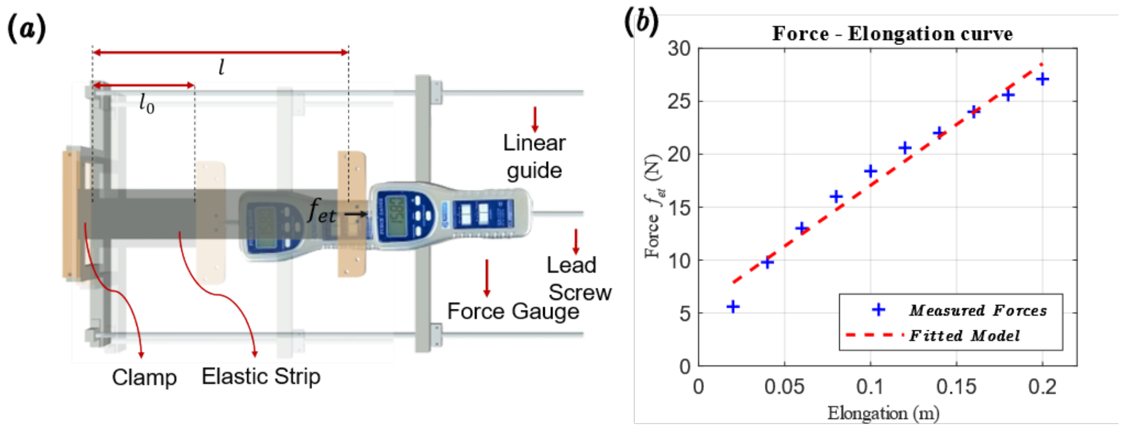

Figure 3.1: (a) Shows the experimental setup to determine the relationship between elastic strip axial force and elongation (b) Depicts the force-elongation relationship measured using (a) for the TheraBand Silver elastic strip (Thickness: 0.5mm). The discrete markers are obtained experimentally, and the dotted line segment shows the linear fit for the experimental data.

0.5mm) and SimpleShot Premium Latex Sheet Elastic Band (Thickness 0.7mm and 1mm), and the force-elongation relationship was determined empirically.

The force-elongation curve shown in Fig.3.1(b) reveals that in the range of displacement between 0 to 100%, the behaviour of the elastic strip remains linear, i.e., $f_{et} = K_e(l - l_0) + C$, where f_{et} is the elastic force, K_e is the elastic constant, l_0 and l are the length at rest and the length of the stretched elastic strip used in the experiment, respectively, and C is the vertical intercept. Therefore, the Hookean behaviour is utilized in the modelling assuming the maximum deflection range within 100% as the operating regime. From the experimental characteristics, the TheraBand Silver (0.5mm thickness) elastic strip was found suitable; hence, it was chosen for further experimentation. The value of $K_e = 114.6$ N/m is obtained from the slope of the curve.

3.1.2 Gripping Force Estimation

The design allows the gripping surface to extend after the contacts have been immobilized and ensures equal tension along the elastic strip's axial direction. A kinematic relationship for the gripper is developed to compute the change in length of the elastic strip while gripping an object using rigid contacts or a fingertip grasp. When the strip is elongated, we parameterize

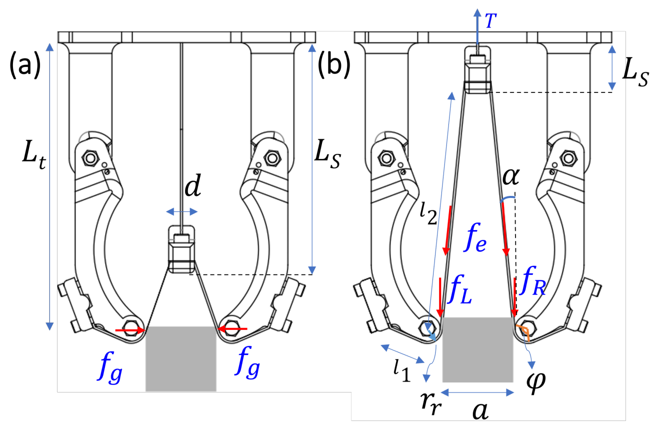

Figure 3.2: Kinematic representation to compute the change in the length of the elastic strip

the length of one-half of the strip as L (refer to Fig. 3.2):

$$L = (l_1 + r_r\phi + \frac{d}{2} + l_2) \tag{3.1}$$

where l_1 is the length from clamping till the common tangent between the roller and elastic strip, r_r is the radius of the roller, ϕ is the central angle of the arc, l_2 is the length from the hoop to the common tangent at the roller, d is the width of the hoop, and a is the width of the grasped object. From the design geometry shown in Fig. 3.2(b), the l_2 segment length can be obtained from:

$$l_2 = \sqrt{\left(\frac{a-d}{2}\right)^2 + (L_t - L_s)^2} \tag{3.2}$$

The lengths L_t and L_s are shown in Fig. 3.2. During grasping, the object makes contact with the flat surface of the elastic substrate by exerting normal contact forces (f_g) at the interaction surface. Since the elastic substrate is assumed to be linearly elastic and isotropic, the elastic force acting on the strip (f_e) is determined by the difference between L_0 and the final elongation L:

$$f_e = K_e(L - L_0) + C \tag{3.3}$$

Where L_0 is the initial half-length of the elastic strip, which is known, and L is obtained from (11). The relationship between the rope tension T and f_e can be expressed as $T = f_e$. The total elastic energy of the strip is assumed to be:

$$V_e = \int_{L_0}^{L} f_e \, dL \tag{3.4}$$

The components of f_e can be resolved into the normal component (f_g) and vertical components (f_L and f_R), where f_L and f_R are the tangential forces at the contacts of the left and right fingers, respectively:

$$f_L = f_R = f_e \cos(\alpha) \tag{3.5}$$

$$f_g = f_e \sin(\alpha) \tag{3.6}$$

where $\alpha = \arctan\left(\frac{(a-d)}{2(L_t-L_s)}\right)$. The assumption is also validated by the experimental results, which are presented next.

3.1.3 Versatile Grasping – Power and Fingertip Grasp

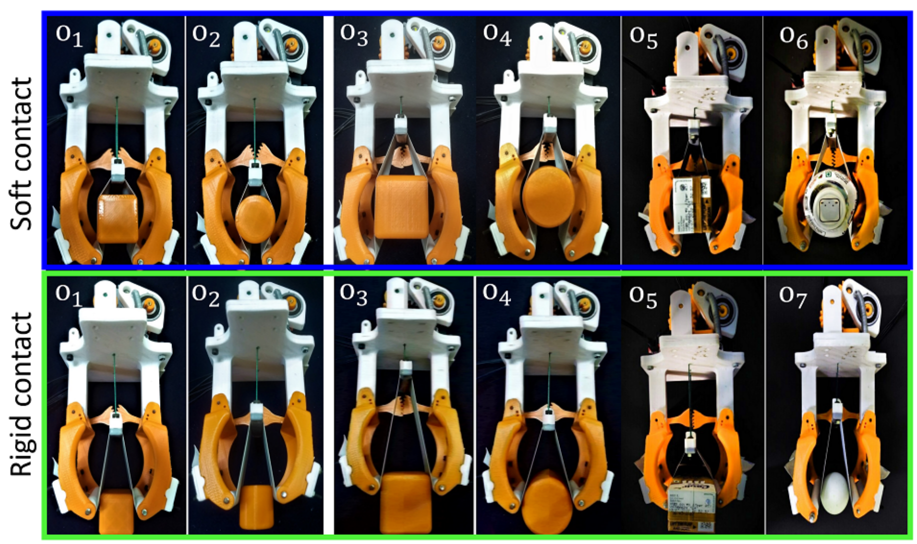

Figure 3.3: Illustrates the capabilities of grasping test objects (o_1 and o_3 – cuboids with sides 35 mm and 50 mm, o_2 and o_4 – cylinder with radius 35 mm and 50 mm, o_5 – tetra pack, o_6 – bottle, and o_7 – egg): 1st row shows soft contact or shape conformation and 2nd row shows rigid contact or fingertip grasp.

A single actuator drives the elastically coupled rigid fingers, making the design simpler and conforming to the object's geometry. The performance was evaluated by grasping objects with different shapes and sizes to demonstrate the gripper's versatility. Figure 3.3 illustrates that the gripper can grasp different 3D printed objects (cuboid with sides 35mm and 50mm, cylinder with radius 35mm and 50mm) by establishing a power grasp (shape conformation) and fingertip grasp. Large deformation of the gripping surface during the power grasp aids the gripper in maintaining a reliable grip even when external disturbances are applied. Compared to traditional two-finger grippers, the proposed gripper can grasp fragile objects through shape conformation and provide safe grasping by adjusting the grasp contact forces. Due to the large contact area and hybrid structure, the frictional force is significantly greater than many rigid grippers. More importantly, the contact force can be modulated by adjusting the stroke length without affecting the contact area between the object and the gripping surface. Due to the hybrid design, the fingertips do not bend if the finger length increases, which is a common issue in many soft grippers.

3.2 Throwing System Modeling

In this section, we present a parametric model of the force impulse applied to the object by the end-effector while throwing and the object dynamics during its projectile motion. In the following description, all poses are expressed with respect to the world coordinate system. The 6-DoF object poses at time t is denoted by ${}^{w}T_o(t)$, with $t = 0$ corresponding to the start of the force application. The model is parameterized by object and end-effector parameters η_o and η_{ee}, respectively. The object state is defined as $q(t) = [{}^{w}T_o(t)\,{}^{w}\dot{T}_o(t)]^T$, where the poses are expressed as a vector of size 7: 3D position and rotation unit quaternion.

3.2.1 Gripping force manipulation

To verify the gripping force f_g determined from the model (16), a setup shown in Fig. 3.4 is developed. The gripping force f_g is modulated by appropriately setting the stroke length L_s while the gripper firmly holds an object, and the corresponding f_g are estimated experimentally. Suppose the coefficient of friction (μ_s) is known, thereby utilizing the Coulomb friction model, the normal contact forces f_g can be estimated from the applied tangential force (f_a'). To measure the coefficient of friction, an object made of PLA material is placed on top of the sample elastic strip with the known vertical load (f_n) and subsequently pulled horizontally using a force gauge with a linear guide using the setup shown in Fig. 3.4(a). Thereby, the friction coefficient is found using

$$\mu_s = \frac{f_a}{f_n}. \tag{3.7}$$

Estimating the torsional coefficient needs the contact geometry as the contact changes; therefore, we assumed that the interaction surface is a planar patch and ignored the torsional

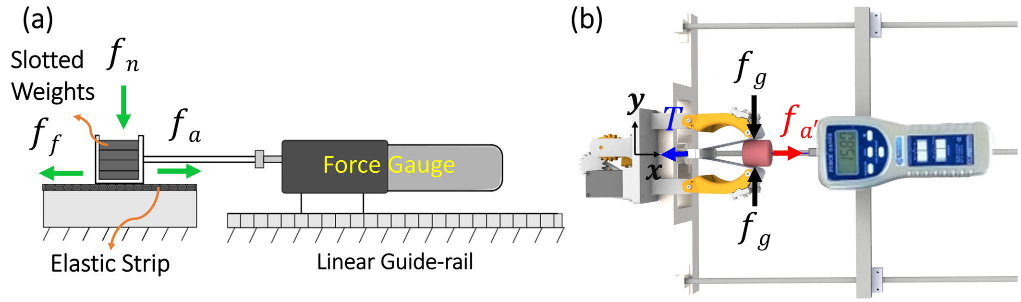

Figure 3.4: Experimental setup to estimate friction coefficient and contact forces: (a) setup to measure the coefficient of friction of between the elastic strip and 3D printed object. (b) setup for estimating the object gripping force.

influence. To estimate f_g during rigid contacts, the gripper is placed along the axis of the linear guide rail, as shown in Fig. 3.4(b). Using static equilibrium conditions, the gripping force required for a stable, rigid grasp is determined using

$$f_g = \frac{f'_a}{2\mu_s} \tag{3.8}$$

where f'_a is the applied force and μ_s is determined experimentally. For each grasp, the object position would reach the centre of the gripper along the y-axis, where the contact forces become equilibrium. It enables the gripper to grasp various objects even with uncertain positions and reduces the likelihood of damaging the object. To demonstrate this, a cylindrical object was considered with two different sizes (35mm, and 50mm). Figure 3.5(a) shows the comparison of f_g estimated using (3.7) from the experiments and the model parameters (3.6) for the fingertip grasp. The closeness of the results also validates the assumption we have considered. Using the same model (3.7), the contact forces during the soft contact are also found experimentally, as shown in Fig. 3.5(b). The plot (refer to Fig. 3.5) shows that the gripping force f_g increases as stroke length decreases. This is expected because reducing the stroke length increases the elastic force, thereby, the gripping force increases. From Fig. 3.5, we can deduce that a greater gripping force is acting on the object of the same diameter and stroke length during soft contact than in rigid contact. This effect is due to more contact area because of shape conformation and the hyperelastic nature of the soft gripping, where the coefficient of friction would be high. From the foregoing, the gripping force estimated from (3.6) is utilized while solving the object dynamics, as detailed next.

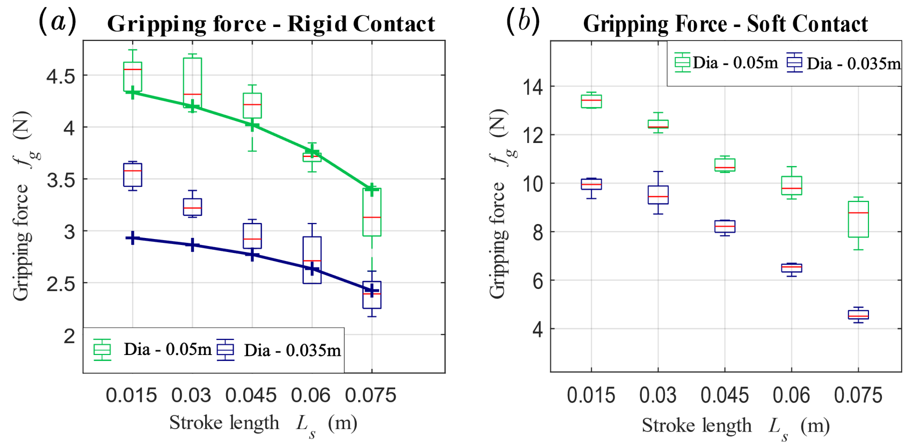

Figure 3.5: Gripping forces (a) compares the experimental data and the estimated using the model for rigid contact (fingertip contact) with the object.(b) experimental data for soft contact with the object.

3.2.2 Elastic Membrane Force

As shown in Fig. 3.6, the elastic band undergoes stretching when setting the stroke length L_s during object grasping. The elongated length, $L(L_s; r_r, l_1, \phi)$, is a function of L_s and the end-effector geometry parameters r_r, l_1, and ϕ, which are shown in Fig. 3.6. Refer to [37] for details about this function. Denoting the initial length of the elastic band by L_0, its deformation is $\Delta L(L_s; r_r, l_1, \phi) = L(L_s; r_r, l_1, \phi) - L_0$. We devised a simplified test setup and derived the following empirical relationship between ΔL and the axial force f_e in the elastic band:

$$f_e = K_{e3}\Delta L^3 + K_{e2}\Delta L^2 + K_{e1}\Delta L + C \tag{3.9}$$

where K_{e3}, K_{e2}, K_{e1}, and C are elasticity parameters. This force is active only for the duration Δt in which the elastic band is in contact with the object. Denoting the set of all end-effector parameters by $\eta_{ee} = \{r_r, l_1, \phi, K_{e3}, K_{e2}, K_{e1}, C, \Delta t\}$, the total magnitude of the force acting on the object is $f_o(L_s; \eta_{ee}) = 2f_e(L_s; \eta_{ee}) \cos\alpha$ (see [37] for details about α). This force acts in the direction shown in Fig. 3.6, in the plane of the end-effector. It can be converted to the world coordinate system using the known end-effector pose. We denote this force generated by the end-effector, represented in the world coordinate system, as the 3D vector ${}^{w}f_o(L_s; \eta_{ee})$.

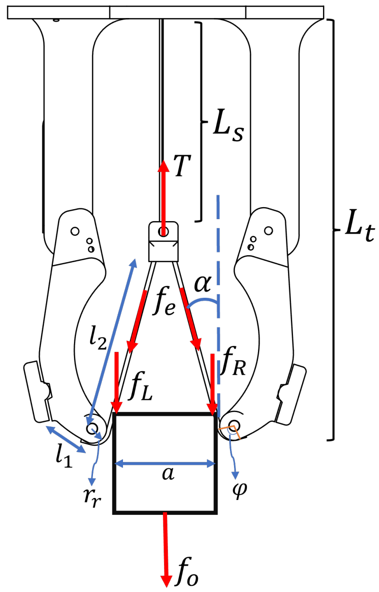

Figure 3.6: Kinematic representation of the end-effector for computing the end-effector's force

3.2.3 Object Dynamics

Having established the initial force applied to the object, the 3D trajectory of the object can be determined through object dynamics. The governing equations of an object's motion, considering the effect of air drag in the world coordinate system, are as follows:

$$\begin{aligned} m\ddot{x} &= {}^{w}f_o(L_s, \tau; \eta_{ee})_x + f_{Dx} \\ m\ddot{y} &= {}^{w}f_o(L_s, \tau; \eta_{ee})_y + f_{Dy} \\ m\ddot{z} &= {}^{w}f_o(L_s, \tau; \eta_{ee})_z + f_{Dz} \\ I_{xx}\dot{\omega}_x + (I_{zz} - I_{yy})\omega_y\omega_z &= 0 \\ I_{yy}\dot{\omega}_y + (I_{xx} - I_{zz})\omega_z\omega_x &= 0 \\ I_{zz}\dot{\omega}_z + (I_{yy} - I_{xx})\omega_x\omega_y &= 0 \end{aligned} \tag{3.10}$$

Where $f_D = f_d + f_g$, with f_d representing the drag force and f_g the force due to gravity, I is the object inertia matrix, and ${}^{w}f_o(L_s, \tau; \eta_{ee})$ is the end-effector force expressed in the world coordinate system. Note that ${}^{w}f_o(L_s, \tau; \eta_{ee})$ is non-zero only during time $\tau \in [0, \Delta t]$, when the elastic potential is being discharged. Denoting the set of object parameters as $\eta_o = \{m, l, b, h\}$ (used to calculate I) and expressing (3.10) as a first-order state space equation:

$$\dot{q}(t) = g(\tau, q(t), L_s; \eta_e, \eta_o) + f_D \tag{3.11}$$

Where g is a nonlinear function describing the object dynamics. This first-order form is used for parameter identification and Throw Optimization (TO).

Equations (3.10) allow determining the object's trajectory for the given initial conditions. In summary, this section reports on the working principle of the different capabilities of the proposed gripper. The next section discusses the mathematical modelling and fabrication of the gripper.

3.3 Prototyping of the End Effector

3.3.1 Design and Fabrication

The end effector, predominantly 3D printed using polylactide polymer (PLA), has been meticulously designed to optimize its functionality and efficiency in performing various tasks. The design emphasizes energy provision through significant displacement of the elastic contact surface, allowing for versatile and effective grasping capabilities.

3.3.2 Elastic Element Selection

Based on the specific task requirements, the characteristics of the elastic element have been selected to maximize elastic energy storage and release. After evaluating various materials, natural latex rubber sheets were identified as the most viable solution due to their superior tensile strength and elongation capabilities. Off-the-shelf natural latex rubber strips with varying thicknesses (0.5mm, 0.7mm, 1mm) were used in the construction and testing of the prototype, allowing for fine-tuning of the gripper's performance based on different experimental needs.

3.3.3 Gripping Surface and Components

The gripping surface of the end effector is made from polyurethane rubber, chosen for its high friction properties, which enhance the grip on various objects. To ensure stability and precision in movement, torsion springs are used to preload the two fingers at their respective pivots.

The spool drum, designed to wind the inextensible thread, features flanges that prevent derailing, ensuring smooth and reliable operation. An encoder attached to the spool drum estimates the gripper's stroke length (L_s), which is critical for accurately controlling the effective wound thread length and, consequently, the gripping force.

3.3.4 Integration and Control

The entire gripper is designed to be compact and lightweight, making it suitable for attachment to floating bases, such as drones, for aerial tasks, including throwing. The gripper is integrated with a Raspberry Pi 4 and a low-level controller for control and measurement purposes. This setup manages the motors and measures the stroke length from the rotary encoder, providing precise control over the gripper's movements.

3.3.5 Prototype Development and Testing

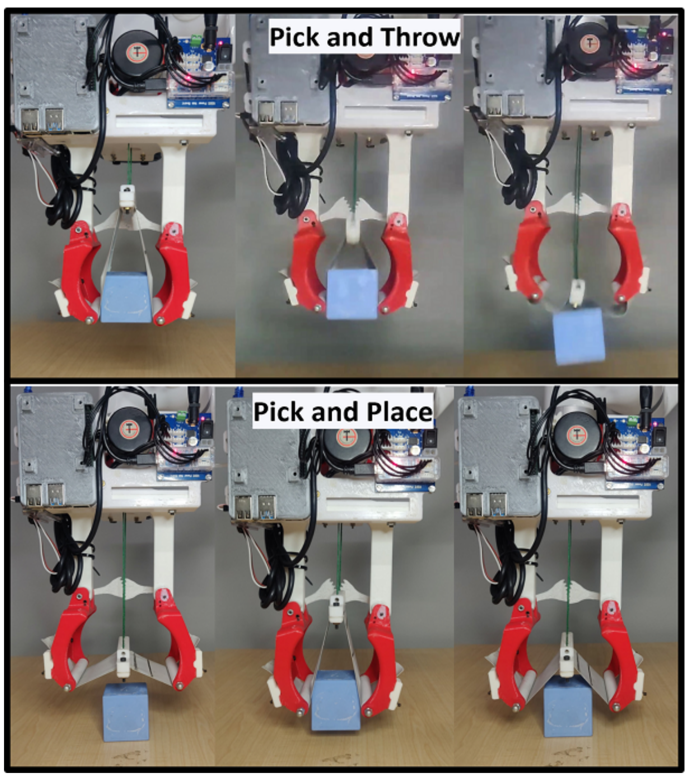

Figure 3.7: Prototype of the end-effector design 2.0

A laboratory prototype of the gripper has been developed, as shown in Fig. 3.7. This prototype serves as a testbed for conducting experimental studies and validating the design's effectiveness. Various tests have been conducted using natural latex rubber strips of different thicknesses to determine the optimal material properties for specific tasks. The experimental results have demonstrated the gripper's ability to perform robust and versatile grasping, confirming the design's suitability for practical applications.

Integrating advanced materials and precise control mechanisms has resulted in a highly functional and adaptable end effector capable of meeting the demands of various challenging tasks.

The current chapter outlines the modeling and prototyping of a versatile end-effector for industrial applications. The chapter begins with a detailed description of the experimental setup used to determine the force-elongation relationship of an elastic strip, revealing a linear behavior within a specific displacement range. This elastic behavior is crucial for the gripper's function, providing the necessary force for secure grasping. The design integrates kinematic relationships to compute changes in the elastic strip's length during gripping, with a focus on achieving both power and fingertip grasps for various objects.

The gripping force is experimentally validated and modeled to ensure reliable performance. Additionally, the chapter discusses the dynamics of the throwing system, including the parametric modeling of force impulse and object trajectory. The prototyping section describes the end effector's design, emphasizing energy provision through elastic elements and precise control mechanisms. Various materials were tested to optimize performance, with natural latex rubber strips proving most effective.

The chapter concludes with the successful development and testing of a laboratory prototype, demonstrating the end effector's capability for robust and versatile grasping. The next chapter will delve into system identification and throw optimization, further refining the end effector's functionality for practical applications.

Chapter 4

Parameter Identification and Throw Optimization

This chapter delves into two critical components for enhancing the accuracy of robotic throwing: parameter identification and throw optimization. Due to the highly sensitive nature of throwing dynamics to model uncertainties, it is essential to accurately estimate both the gripper's and the object's parameters. The chapter presents a comprehensive two-stage parameter identification process to minimize the discrepancies between observed and predicted trajectories. It addresses the throw optimization problem, aiming to find the optimal initial conditions and control variables to achieve precise target locations. The integration of these methodologies forms the backbone of the approach to dynamic and accurate object manipulation in robotics.

4.1 Parameter Identification

The dynamics of throwing are highly sensitive to uncertainties in both the gripper's model and the object's model parameters. Even minor discrepancies can significantly affect the object's trajectory and final position. Accurately modelling the interaction between the gripper and the object is challenging. To approximate the relationship between the object's final location ($\mathbf{p}_g$) and the gripper's control variable (L_s) with high fidelity, we exploit the coupled nature of the gripper model and the object's dynamics, as detailed in Algorithm 1.

We perform a two-stage parameter identification process:

1. **Gripper Model Parameters ($\boldsymbol{\eta}$):** The gripper model parameters are estimated by minimizing the error norm between the experimentally observed final reach ($\mathbf{x}_e$) and the computed reach from the mathematical model ($\mathbf{x}_m$). The gripper parameters include $K_{e1}, K_{e2}, K_{e3}, C$ as defined in (3.9), and r_r, l_1, ϕ obtained from the geometry of the grip-

per. A set of N samples is collected using various sample objects (cylinder, cuboid, and cube) thrown at different ranges with different stroke lengths.

2. **Object Model Parameters (o*):** Using the optimal gripper parameters ($\boldsymbol{\eta}^*$) obtained from Stage 1, the object's parameters (m, l, b, h)—representing the mass, length, breadth, and height of the object, respectively—are estimated.

Algorithm 1 is employed to identify and incorporate these parameters into the model. Figure 4.3 demonstrates the improved accuracy of the model after incorporating $\boldsymbol{\eta}^*$ and $\boldsymbol{\xi}^*$, showing a significant enhancement in the closeness between the experimentally estimated and system model predicted reaches.

To predict the target location of the object, we integrate the object's dynamics forward in time from Equation (3.10) until $z = 0$, where the object hits the ground plane. This requires knowledge of the object and end-effector parameters ($\boldsymbol{\eta}_o$ and $\boldsymbol{\eta}_{ee}$, respectively). Given the dynamic nature of throwing, even small errors in these parameters can lead to substantial deviations in the predicted target location ($\mathbf{p}_m(L_s; \boldsymbol{\eta}_o, \boldsymbol{\eta}_{ee})$). Thus, we develop the parameter identification algorithm.

In our iterative two-stage algorithm (Algorithm 1), N denotes the number of data points, p_{obs} the observed landing location, and K the number of objects. The process involves:

1. Initializing $\boldsymbol{\eta}_o^{(j)}$ from CAD models and minimizing the L_2 distance between the experimentally observed final reach of the object and its model-based estimate. This updates the end-effector parameters $\boldsymbol{\eta}_{ee}$, which are consistent across all K objects.

2. Using the updated $\boldsymbol{\eta}_{ee}$ from Stage 1 in the same objective function to update the K object parameters $\{\boldsymbol{\eta}_o^{(j)}\}_{j=1}^{K}$.

These stages are repeated until convergence, i.e., until the changes in the end-effector and object parameters between iterations fall below a specified threshold.

4.1.1 Assessment of Parameter Identification

We assess the effectiveness of the parameter identification (PI) process described in the above section 4.1 by comparing the observed reach of the thrown object with the reach predicted by the mathematical model. Reach is calculated as the component of the 3D landing location along the axis straight ahead of the robot.

Figures 4.1 & 4.2 show that the reach prediction accuracy of the model increases significantly after PI for all the objects considered. Specifically, Figure 4.3 compares the throw reach

Algorithm 1: Parameter Identification

Inputs:

- Dataset: (object target location, stroke length, object ID) $\{\left(\mathbf{p}_{obs}^{(i)}, L_s^{(i)}, o^{(i)}\right)\}_{i=1}^{N}$.
- Initial end-effector parameters $\boldsymbol{\eta}_{ee,init}$.
- Initial object parameters $\{\boldsymbol{\eta}_{o,init}^{(j)}\}_{j=1}^{K}$ from CAD models.

Output: Optimized parameters $\boldsymbol{\eta}_{ee}^{*}$, $\{\boldsymbol{\eta}_{o}^{(j)*}\}_{j=1}^{K}$

Initialization:

$\boldsymbol{\eta}_{ee} \leftarrow \boldsymbol{\eta}_{ee,init}$

for $j = 1$ ***to*** K **do**

  $\boldsymbol{\eta}_{o}^{(j)} \leftarrow \boldsymbol{\eta}_{o,init}^{(j)}$

end

repeat

  Stage 1:

$$\boldsymbol{\eta}_{ee} = \arg\min_{\boldsymbol{\eta}_{ee}} \sum_{i=1}^{N} ||\mathbf{p}_m(L_s^{(i)}; \boldsymbol{\eta}_o^{(o^{(i)})}, \boldsymbol{\eta}_{ee}) - \mathbf{p}_{obs}^{(i)}||_2^2$$

  Stage 2: **for** $j = 1$ ***to*** K **do**

$$\boldsymbol{\eta}_o^{(j)} = \arg\min_{\boldsymbol{\eta}_o} \sum_{i \in \mathcal{N}_j} ||\mathbf{p}_m(L_s^{(i)}; \boldsymbol{\eta}_o^{(j)}, \boldsymbol{\eta}_{ee}) - \mathbf{p}_{obs}^{(i)}||_2^2$$

  end

until *change in* $\boldsymbol{\eta}_{ee}$ *or* $\{\boldsymbol{\eta}_o^{(j)}\}_{j=1}^{K}$ *is less than threshold*;

$\boldsymbol{\eta}_{ee}^{*} \leftarrow \boldsymbol{\eta}_{ee}$

for $j = 1$ ***to*** K **do**

  $\boldsymbol{\eta}_o^{(j)*} \leftarrow \boldsymbol{\eta}_o^{(j)}$

end

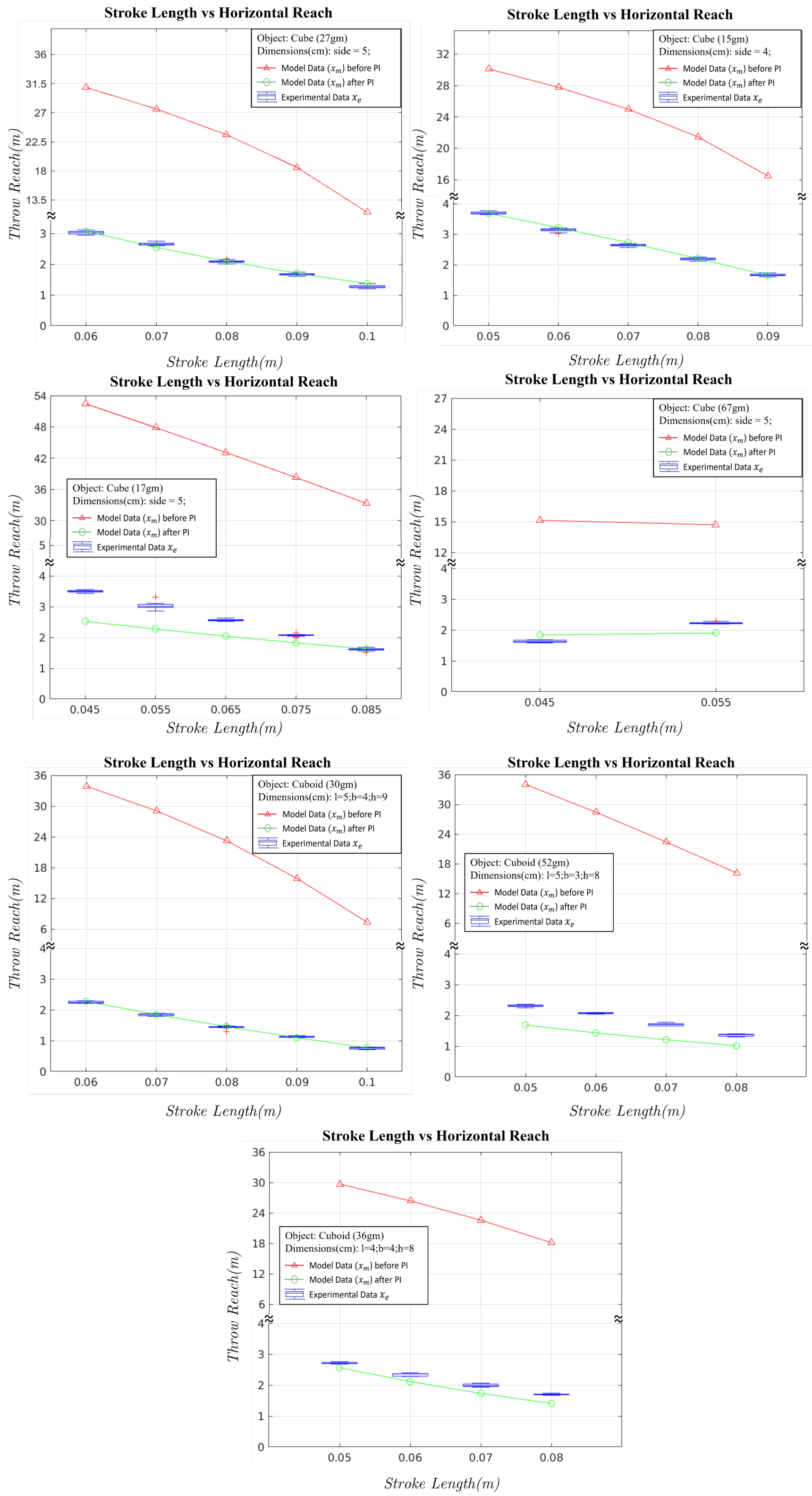

Figure 4.1: Illustrates the comparison between the throw reach of 4 different cubes and 3 different cuboids obtained from the mathematical model before and after performing parameter identification. The boxplot shows the experimental horizontal reach of the considered object.

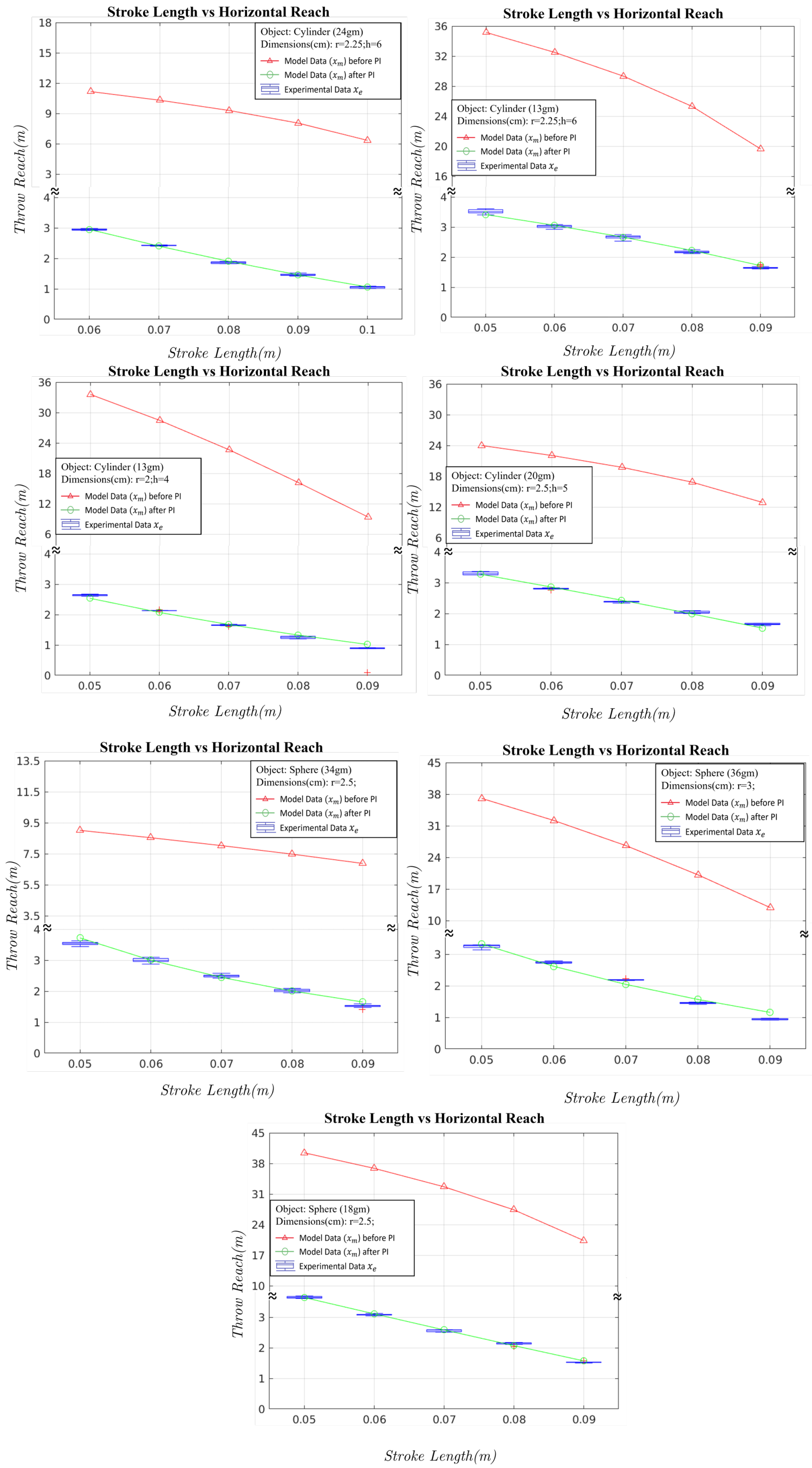

Figure 4.2: Illustrates the comparison between the throw reach of 4 different cylinders and 3 different spheres obtained from the mathematical model before and after performing parameter identification. The boxplot shows the experimental horizontal reach of the considered object.

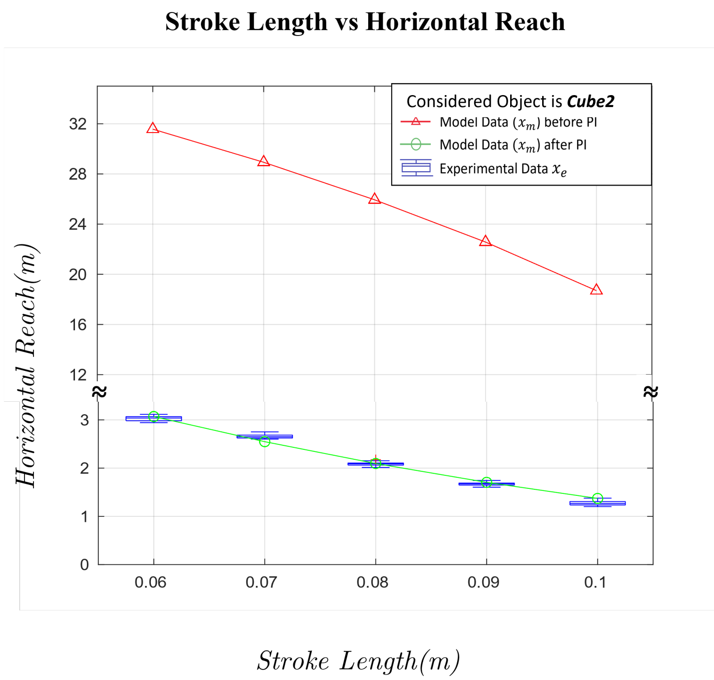

Figure 4.3: Illustrates the comparison between the throw reach of a cube obtained from the mathematical model before and after performing parameter identification. The boxplot shows the experimental horizontal reach of the cube.

for a cube of side 5 cm before and after PI (refer to the supplementary material for the plots of other objects considered for PI). It is important to note the limitations of PI, which lead to inaccuracies when throwing unseen objects to the target location. This occurs because the end-effector (EE) and model parameters are not updated within the throw optimization (TO) settings, as detailed in Section 4.2.

To address this issue, we adopt residual learning techniques as detailed in Chapter 5, and the outcomes are elaborated in the subsequent sections.

4.2 Throw Optimization

To achieve the desired target location $\mathbf{p}_{des}$, we solve a constrained nonlinear optimization problem to determine the optimal initial state $\mathbf{q}(0)^*$ and the stroke length L_s^*:

$$\begin{aligned} \mathbf{q}(0)^*, L_s^* = \arg \min_{\mathbf{q}(0), L_s} & ||\mathbf{p}_m(L_s; \boldsymbol{\eta}_o^*, \boldsymbol{\eta}_{ee}^*) - \mathbf{p}_{des}||_2^2 \\ \text{s.t.} \quad & \text{Eq. (3) (object dynamics)}, \\ & \mathbf{q}(0)_{min} \leq \mathbf{q}(0) \leq \mathbf{q}(0)_{max}, \\ & L_{s,min} \leq L_s \leq L_{s,max} \end{aligned} \tag{4.1}$$

Here, $\boldsymbol{\eta}^*_{ee}$ and $\boldsymbol{\eta}^*_o$ are the identified end-effector and object parameters, respectively. The limits for the initial state $(\mathbf{q}(0)_{min}, \mathbf{q}(0)_{max})$ and stroke length $(L_{s,min}, L_{s,max})$ are determined based on the robot's operating environment and the end-effector dimensions.

Once the optimal initial state $\mathbf{q}(0)^*$ and L^*_s are obtained, the robot plans a secondary trajectory to reach the end-effector pose. The throwing event is executed once the robot reaches these optimal initial conditions.

The nonlinear constrained optimization technique finds the initial condition $\boldsymbol{\sigma}$ for placing the object at the desired location. The decision variable $\boldsymbol{\sigma}$ is defined as follows:

$$\boldsymbol{\sigma} = [x, y, z, \dot{x}, \dot{y}, \dot{z}, \phi, \theta, \psi, L_s]^T \tag{4.2}$$

Here, x, y, z represents the initial position of the object's center of mass, $\dot{x}, \dot{y}, \dot{z}$ represents the initial velocity of the object, ϕ, θ, ψ represent the object's orientation with respect to the $\mathcal{F}$ frame, and L_s is the stroke length control variable. The initial velocity $[\dot{x}, \dot{y}, \dot{z}]^T$ for a fixed base is assumed to be zero, thus eliminating the need for acceleration and deceleration phases to launch the object. However, the initial velocities are treated as free variables for a moving base.

The throw optimization problem, which is equivalent to the trajectory optimization problem, is defined as follows:

- **Goal Position:** $\mathbf{p}_g = [x_g, y_g, z_g]^T$
- **Decision Variable:** $\boldsymbol{\sigma} = [x, y, z, \dot{x}, \dot{y}, \dot{z}, \phi, \theta, \psi, L_s]^T$
- **Objective Function:**

$$\min_{\boldsymbol{\sigma}} ||\mathbf{p}_g - \mathbf{p}||_2^2 \tag{4.3}$$

- **Subject to:**

$$\dot{\mathbf{p}} = \mathbf{f}(\mathbf{q}) + \mathbf{g}(L_s, \tau) \quad \text{(Object dynamics)} \tag{4.4}$$

$$\boldsymbol{\sigma}_L < \boldsymbol{\sigma} < \boldsymbol{\sigma}_U \quad \text{(Boundary conditions)} \tag{4.5}$$

Here, $\boldsymbol{\sigma}_U$ and $\boldsymbol{\sigma}_L$ are the upper and lower bounds for the variable $\boldsymbol{\sigma}$. Once the optimal initial condition $\boldsymbol{\sigma}^*$ is obtained from the throw optimization, the mobile manipulator plans the secondary trajectory to reach the gripper's pose with nonzero velocity. The robot then executes the throw upon reaching the optimal initial position.

This chapter focuses on improving the accuracy of throwing dynamics by addressing uncertainties in both gripper and object models. The parameter identification (PI) process is detailed through a two-stage algorithm to estimate gripper and object model parameters by minimizing the error between observed and model-predicted object reaches. The effectiveness of PI is assessed by comparing the accuracy of reach predictions before and after parameter identification. Furthermore, the throw optimization problem is formulated as a constrained nonlinear optimization task to determine the optimal initial state and stroke length for achieving a desired target location. The next chapter highlights the need to integrate throw optimization with learning-based approaches to further address limitations and enhance accuracy.

Chapter 5

Learning Based Control

In this chapter, the integration of learning-based control techniques for enhancing the accuracy and repeatability of targeted throwing tasks is explored. Beginning with the collection of experimental data, which involved capturing manipulator movements and calibrating cameras to obtain precise object pose data, the chapter proceeds to discuss the implementation of residual learning methodologies. Various machine learning algorithms are assessed for their effectiveness in predicting stroke length adjustments (ΔL_s), with support vector regression (SVR) emerging as the most suitable approach.

The targeted throwing process, facilitated by throw optimization and SVR-based residual learning, is then detailed. This process enables accurate throwing of unseen objects to specified target locations, showcasing the system's adaptability and precision. Finally, repeatability tests conducted on both robot arm and drone platforms demonstrate the system's consistent performance across multiple trials under various conditions, underscoring its reliability and robustness.

5.1 Data Collection

Our experimental setup involved varying stroke lengths (L_s) as measured by an encoder in the end-effector and conducting throws of sample objects, including cubes, spheres, and cylinders of various sizes and masses. Data collection was conducted by setting the EE's pose and capturing images of the manipulator during experiments, with a camera positioned to provide a lateral view of the manipulator's movement and a checkerboard placed in the ackground to be considered as the reference plane. We perform camera calibration to obtain extrinsic and intrinsic parameters, along with the offset between the checkerboard and the plane of the object's trajectory. Next, we identify the object's centre pixel coordinates from each captured image. Finally, we calculate the object's world coordinates by utilizing the known offsets and camera parameters. This pose data was then utilized to determine the reach of the thrown object. Our final dataset consists of 865 throws of 14 objects, such as cubes, cylinders, spheres, and cuboids. These objects were selected to represent different dimensions and masses.

5.2 Residual Learning

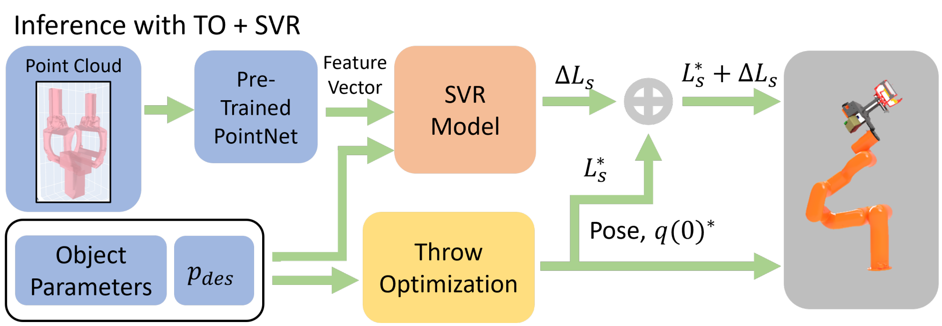

Figure 5.1: Illustrates the methodology describing the end-to end operations from the given input parameters to applying motion commands to the robots.

The effectiveness of residual learning is assessed by the accuracy of ΔL_s prediction. Out of the 14 objects comprising our dataset, as discussed in Section 5.1, we held out two objects in a round-robin fashion and trained on the remaining 12 objects. The mean and standard deviation of the mean square prediction error are computed over all the training runs as shown in Table 5.1.

We tried the following learning algorithms: multi-layer perceptron (MLP) neural network, random forest (RF), and support vector regression (SVR). The MLP considered in this context is a three-layered network that takes in the feature vector extracted from a pre-trained PointNet architecture [39] and the object parameters as input to give the residual stroke length (ΔL_s). Table 5.1 shows that in our low-data regime, the MLP underperforms due to low data and overfits on the seen data, whereas the SVR model performs best. Hence, all the throw experiments described after this are conducted with the SVR residual learning model.

Table 5.1: Comparison of machine learning algorithms for residual learning (error in ΔL_s prediction). The mean square error (MSE) is computed between the predicted and calculated ΔL_s.

Residual Learning Algorithm	**ΔL_s MSE (mm)**
Multi-layer Perceptron (MLP)	610.5039 ± 268.2805
Random Forest (RF)	0.2082 ± 0.1334
Support Vector Regression (SVR)	**0.2056 ±0.1146**

5.3 Targeted Throwing

In this subsection, we evaluate the ability of our entire system to throw a given object to a specified target location. We used unseen objects (see object shapes presented in Fig. 5.2) that are distinct from those used for parameter identification and residual model training. Specifically, we used 5 non-convex and 2 primitive shapes (a cube and a cuboid of unseen mass and dimensions). We conducted 5 throws per object using the following procedure (depicted in Fig. 5.1) to throw a given object to a specified target location. First, we calculate the end-effector pose $q(0)$ and stroke length L_s using throw optimization. The object mass is assumed to be known, and the inertia matrix is calculated from the CAD software. Next, we compute the object surface point cloud from the mesh and use the composite point cloud as shown in Fig.5.3 to calculate the residual stroke length. Finally, we ensure that the object roughly matches the pose taken in the mesh file and set the end-effector stroke length to $L_s + \Delta L_s$, following which a flag is transmitted to the controller to initiate the throwing event. The object takes a flight trajectory and ultimately lands on the ground. The landing location is recorded and compared with the target landing location.

Figure 5.2 shows that our throw optimization algorithm, in conjunction with SVR-based residual learning, is able to throw all the unseen objects with reasonable accuracy near their specified target locations. Residual learning significantly increases throw accuracy. We observe that model-based throw optimization tends to overshoot the target, possibly because it does not account for the extra stretching of the elastic band induced by the complex-shaped objects. Residual learning overshoots much less, possibly because it is trained to predict ΔL_s based on the object shape and its location within the end-effector grip.

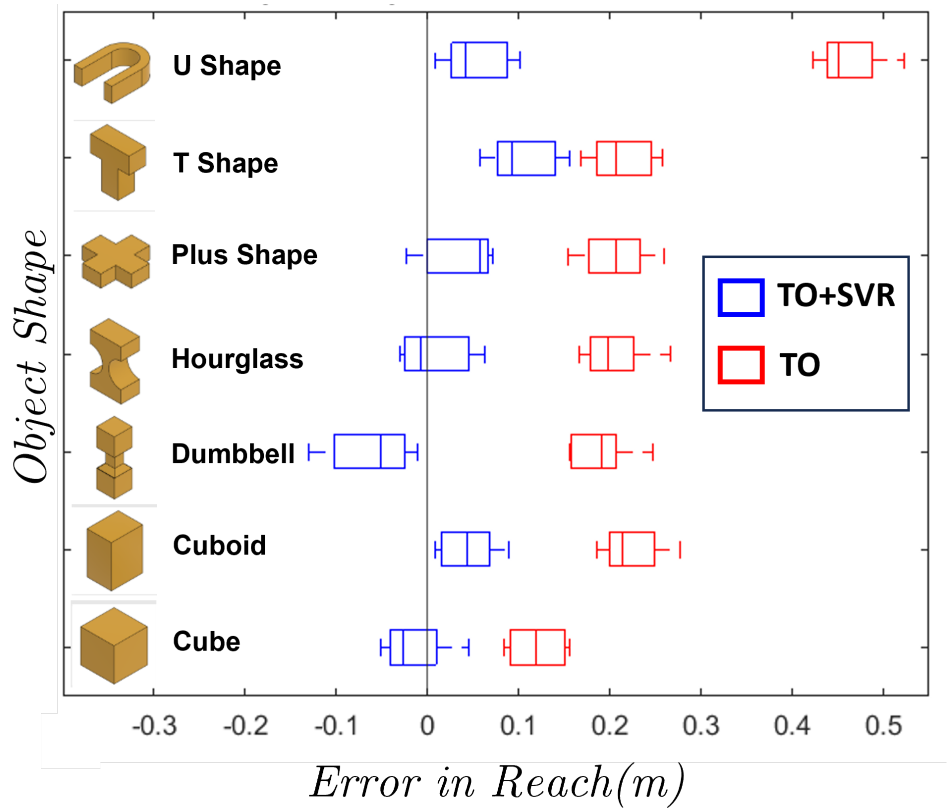

Figure 5.2: Illustration of the comparison between the throw reach of a cube obtained from the mathematical model before and after performing parameter identification. The boxplot shows the experimental horizontal reach of the cube.

5.3.1 Repeatability of Targeted Throwing

A preliminary assessment of the repeatability of the targeted throwing ability of our end-effector on two platforms: a robot arm and a drone. Different from accuracy, this tests how closely the object lands over multiple trials for a given stroke length.

When mounted on the robot arm and throwing a cube with a side length of 5 cm, the observed reach was 1.345 ± 0.1086 m over 20 trials.

When mounted on a drone and throwing the same cube, we conducted 20 trials with the same stroke length for four different propeller speeds to test the effect of propeller wash. The observed reach was 3.046 ± 0.0941 m, 3.0387 ± 0.0949 m, 2.832 ± 0.0955 m, and 2.8221 ± 0.1003 m for propeller speeds of 0, 8900, 13900, and 14860 RPM respectively.

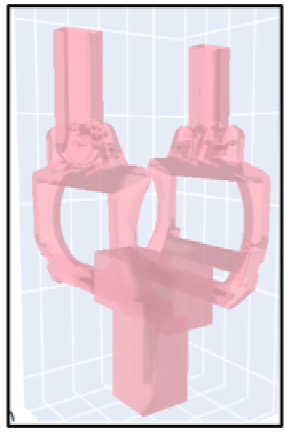

Figure 5.3: The point cloud of the end-effector's fingers grasping an object is used as one of the inputs to the residual network.

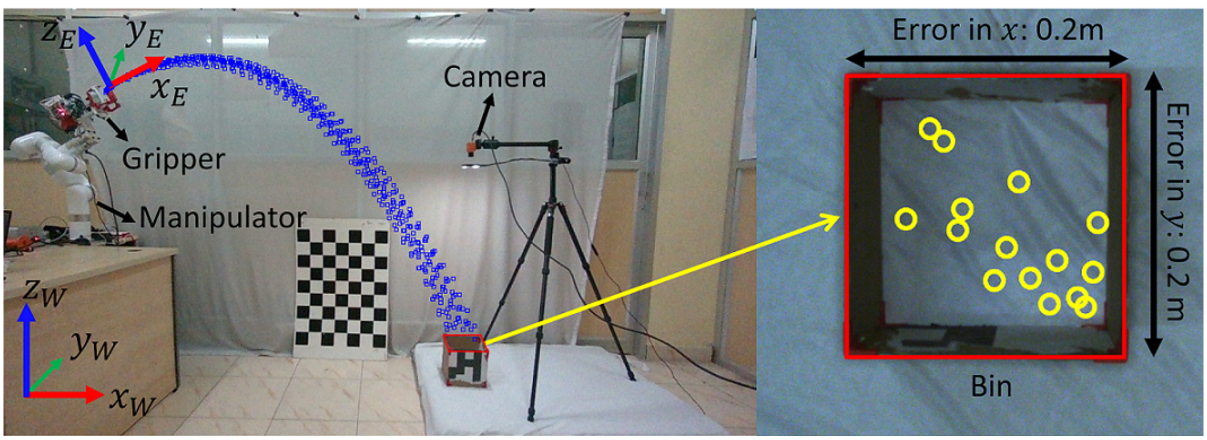

Figure 5.4: Repeatability of the throwing end-effector integrated with a manipulator

Platform	**Propeller Speed (RPM)**	**Reach (m)**
Robot Arm	N/A	1.345 ± 0.1086
Drone	0	3.046 ± 0.0941
	8900	3.0387 ± 0.0949
	13900	2.832 ± 0.0955
	14860	2.8221 ± 0.1003

Table 5.2: Repeatability of targeted throwing on different platforms.

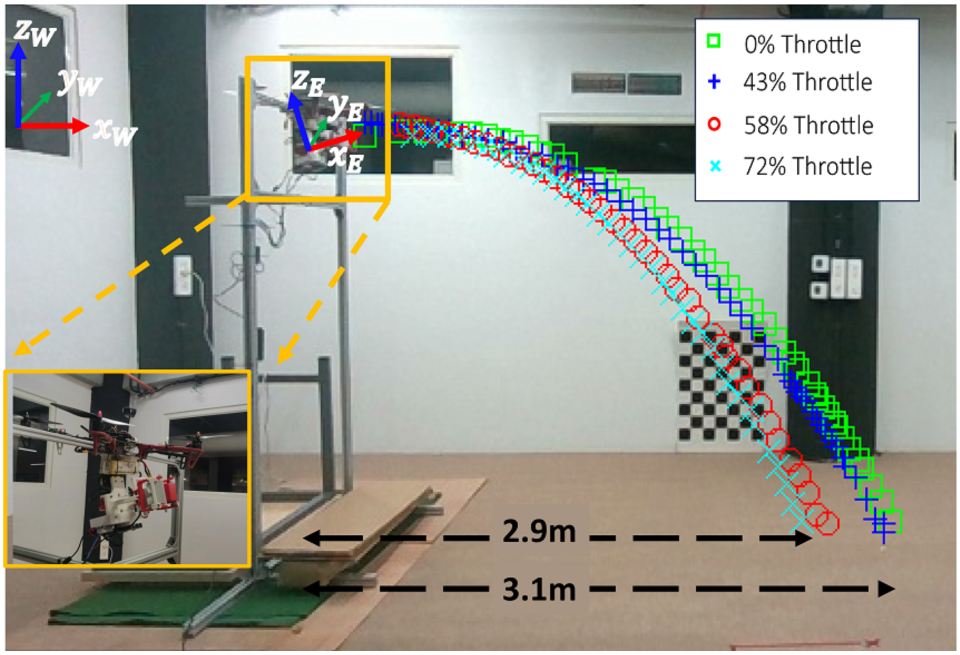

Figure 5.5: Repeatability of the throwing end-effector integrated with drone

These results indicate that while the accuracy of the throw can vary depending on the platform and conditions such as propeller speed, the system exhibits good repeatability under consistent conditions.

The chapter outlines the methodology and results of utilizing machine learning techniques to enhance the accuracy and repeatability of targeted throwing tasks. Data collection involved capturing images of the manipulator's movements and calibrating the camera to obtain object pose data. Residual learning, assessed through various machine learning algorithms, effectively predicted stroke length adjustments (ΔL_s). Support vector regression (SVR) emerged as the best-performing algorithm for this task. The targeted throwing process involved employing throw optimization coupled with SVR-based residual learning to accurately throw unseen objects to specified target locations. Repeatability tests conducted on a robot arm and a drone demonstrated consistent performance across multiple trials, indicating the system's reliability under various conditions.

Chapter 6

Conclusion

In this thesis, we have introduced a significant advancement in robotic manipulation through the development of a novel two-DoF gripper, inspired by the mechanics of a slingshot. This innovative design offers a versatile approach to object handling, enabling the gripper to pick, place, or dynamically throw objects to designated locations. The core of our design is the use of an elastic membrane as a gripping surface, which is activated through a latching mechanism to store elastic potential energy. The controlled release of this energy determines whether an object is gently placed or swiftly propelled towards its target.

We implemented a throw optimization technique to calculate the initial parameters required for targeted throws. However, the inherent dynamics of throwing introduce uncertainties due to variations in model or environmental parameters, which can affect accuracy. To mitigate these challenges, we developed a comprehensive two-stage parameter identification process. This iterative refinement method has significantly improved our ability to reach desired goal locations, as demonstrated through experimental validation. To further address the uncertainties in the object's reach, we incorporated a residual learning algorithm along with throw optimization. This combination reduces the effects of unmodeled dynamics and enables the system to accurately throw unseen objects to target locations.

Our experiments have highlighted the remarkable capabilities of the proposed gripper, both in standalone operations and when integrated with robotic platforms such as manipulators and drones. Notably, the end-effector has demonstrated the ability to project objects well beyond the traditional manipulation workspace, indicating its potential for applications requiring extended reach and dynamic object manipulation.

Looking ahead, there are several exciting avenues for future work. One promising direction is the development of an updated version of the end-effector that can catch, grasp, pick, and throw objects. Integrating this enhanced gripper with various robotic systems could enable it to perform tasks with non-zero initial velocities, such as catching or transferring objects between robots. This capability would be particularly useful in scenarios where two robots need to transfer an object from one to another, adding a new dimension to collaborative robotic manipulation.

Furthermore, scaling the design appropriately holds promise for enhancing reach capabilities, opening up possibilities for a wide range of practical applications. By continuing to refine and optimize the gripper design and control algorithms, we envision even greater advancements in robotic manipulation, with significant implications across various industries and domains.

In conclusion, this thesis represents a contribution to the field of robotics, offering a transformative approach to object manipulation through the development of this innovative end-effector. With its unique design, advanced control mechanisms, and demonstrated capabilities, the end-effector sets a new standard for how robots interact with and manipulate objects in diverse real-world scenarios. The future work proposed here will further enhance its functionality and broaden its applicability, paving the way for more sophisticated and versatile robotic systems.

Chapter 7

Related Publications

1. **Identification and Learning-Based Control of an End-Effector for Targeted Throwing**
   Pasala Haasith Venkata Sai, Nagamanikandan Govindan, Samarth Brahmbhatt
   IEEE Robotics and Automation Letters (Under-Review)

2. **A Novel Hybrid Gripper Capable of Grasping and Throwing Manipulation**
   Nagamanikandan Govindan, Bharadhwaj Ramachandran, **Pasala Haasith Venkata Sai**, K. Madhava Krishna
   IEEE/ASME Transactions on Mechatronics, vol. 28, no. 6, pp. 3317-3328

Bibliography

[1] Gal Ribak, Oded Mordechay, and Daniel Weihs. Why are there no long distance jumpers among click-beetles (elateridae)? *Bioinspiration Biomimetics*, 8(3):036004, jul 2013.

[2] Stephen M. Deban, J. C. O'Reilly, Ulrike Dicke, and J. L. Van Leeuwen. Extremely high-power tongue projection in plethodontid salamanders. *Journal of Experimental Biology*, 210(4):655–667, feb 2007.

[3] Sheila N. Patek, Joseph E. Baio, Brian L. Fisher, and Andrew V. Suarez. Multifunctionality and mechanical origins: Ballistic jaw propulsion in trap-jaw ants. *Proceedings of the National Academy of Sciences*, 103(34):12787–12792, aug 2006.

[4] Alexander Sakes, Michiel Der Van Wiel, Peter W. J. Henselmans, Johan L. Van Leeuwen, Dimitrios Dodou, and Pieter Breedveld. Shooting mechanisms in nature: A systematic review. *PLoS ONE*, 11(7):1–46, jul 2016.

[5] Jonghoon Kim. Optimization of throwing motion planning for whole-body humanoid mechanism: Sidearm and maximum distance. *Mechanism and Machine Theory*, 46(4):438–453, apr 2011.

[6] Kade D. Feller, Gregory P. Sutton, and Pablo T. Gonzalez-Bellido. Medium compensation in a spring-actuated system. *Journal of Experimental Biology*, 223(4):1–5, feb 2020.

[7] S. Divi et al. Latch-based control of energy output in spring actuated systems. *Journal of the Royal Society Interface*, 17(168), jul 2020.

[8] C. Piazza, G. Grioli, M.G. Catalano, and A. Bicchi. A century of robotic hands. *Annual Review of Control, Robotics, and Autonomous Systems*, 2(Volume 2, 2019):1–32, 2019.

[9] Aude Billard and Danica Kragic. Trends and challenges in robot manipulation. *Science*, 364(6446):eaat8414, 2019.

[10] Matthew T. Mason. Toward robotic manipulation. *Annual Review of Control, Robotics, and Autonomous Systems*, 1(Volume 1, 2018):1–28, 2018.

[11] Antonio Bicchi. Hands for dexterous manipulation and robust grasping: a difficult road toward simplicity. *IEEE Trans. Robotics Autom.*, 16:652–662, 2000.

[12] J. S. Hu, M. C. Chien, Y. J. Chang, S. H. Su, and C. Y. Kai. A ball-throwing robot with visual feedback. In *IEEE/RSJ 2010 International Conference on Intelligent Robots and Systems, IROS 2010 - Conference Proceedings*, pages 2511–2512, 2010.

[13] T. Senoo, A. Namiki, and M. Ishikawa. High-speed throwing motion based on kinetic chain approach. In *2008 IEEE/RSJ International Conference on Intelligent Robots and Systems, IROS*, pages 3206–3211, 2008.

[14] F. Lombai and G. Szederkényi. Throwing motion generation using nonlinear optimization on a 6-degree-of-freedom robot manipulator. In *IEEE 2009 International Conference on Mechatronics, ICM 2009*, volume 00, pages 17–22, 2009.

[15] Y. Zhang, J. Luo, and K. Hauser. Sampling-based motion planning with dynamic intermediate state objectives: Application to throwing. In *Proc IEEE Int Conf Robot Autom*, pages 2551–2556, 2012.

[16] Amir Sintov and Amir Shapiro. A stochastic dynamic motion planning algorithm for object-throwing. In *Proc IEEE Int Conf Robot Autom*, volume 2015-June, pages 2475–2480, 2015.

[17] A. Zeng, S. Song, J. Lee, A. Rodriguez, and T. Funkhouser. Tossingbot: Learning to throw arbitrary objects with residual physics. In *Robotics: Science and Systems*, 2019.

[18] H. Arisumi, K. Yokoi, T. Kotoku, and K. Komoriya. Study on casting manipulation (2nd report, experiments of swing control and gripper throwing). *Nihon Kikai Gakkai Ronbunshu, C Hen/Transactions of the Japan Society of Mechanical Engineers, Part C*, 65(639):4356–4363, 1999.

[19] J. H. Choi, K. Nam, and S. Oh. High-accuracy driving control of a stone-throwing mobile robot for curling. *IEEE Transactions on Automation Science and Engineering*, 2021.

[20] H. Frank, A. Mittnacht, T. Moschinsky, and F. Kupzog. 1-dof-robot for fast and accurate throwing of objects. In *ETFA 2009 - 2009 IEEE Conference on Emerging Technologies and Factory Automation*, 2009.

[21] T. Mouri, H. Kawasaki, K. Yoshikawa, J. Takai, and S. Ito. Anthropomorphic robot hand: Gifu hand iii. In *International Conference on Control, Automation and Systems*, pages 1288–1293, 2002.

[22] C. Gosselin, F. Pelletier, and T. Laliberte. An anthropomorphic underactuated robotic hand with 15 dofs and a single actuator. In *2008 IEEE International Conference on Robotics and Automation*, pages 749–754, May 2008.

[23] Y. Hao et al. A multimodal, enveloping soft gripper: Shape conformation, bioinspired adhesion, and expansion-driven suction. *IEEE Transactions on Robotics*, 37(2):350–362, apr 2021.

[24] A. A. Stokes, R. F. Shepherd, S. A. Morin, F. Ilievski, and G. M. Whitesides. A hybrid combining hard and soft robots. *Soft Robotics*, 1(1):70–74, 2014.

[25] A. Firouzeh and J. Paik. Grasp mode and compliance control of an underactuated origami gripper using adjustable stiffness joints. *IEEE/ASME Transactions on Mechatronics*, 22(5):2165–2173, oct 2017.

[26] R. R. Ma, W. G. Bircher, and A. M. Dollar. Toward robust, whole-hand caging manipulation with underactuated hands. In *Proceedings - IEEE International Conference on Robotics and Automation*, pages 1336–1342. IEEE, may 2017.

[27] L. U. Odhner, Aaron M. Dollar, K. Matl, and Danica Kragic. A compliant, underactuated hand for robust manipulation. *The International Journal of Robotics Research*, 33(7):736–752, 2014.

[28] R. R. Ma, N. Rojas, and A. M. Dollar. Spherical hands: Toward underactuated, in-hand manipulation invariant to object size and grasp location. *Journal of Mechanical Robotics*, 8(6):061021, nov 2016.

[29] L. Cao, A. T. Dolovich, A. L. Schwab, J. L. Herder, and W. (Chris) Zhang. Toward a unified design approach for both compliant mechanisms and rigid-body mechanisms: Module optimization. *Journal of Mechanical Design*, 137(12):1–10, dec 2015.

[30] G. Hao, H. Li, A. Nayak, and S. Caro. Design of a compliant gripper with multimode jaws. *Journal of Mechanical Robotics*, 10(3):031005, mar 2018.

[31] A. J. Spiers, B. Calli, and A. M. Dollar. Variable-friction finger surfaces to enable within-hand manipulation via gripping and sliding. *IEEE Robotics and Automation Letters*, 3(4):4116–4123, oct 2018.

[32] J. R. Amend, E. Brown, N. Rodenberg, and H. M. Jaeger. A positive pressure universal gripper based on the jamming of granular material. *IEEE Transactions on Robotics*, 28(2):341–350, 2012.

[33] Y. Liu, A. Nayak, and A. Billard. A solution to adaptive mobile manipulator throwing. In *2022 IEEE/RSJ International Conference on Intelligent Robots and Systems (IROS)*, pages 1625–1632, 2022.

[34] A. Ghadirzadeh, A. Maki, D. Kragic, and M. Bjorkman. Deep predictive policy training using reinforcement learning. In *IEEE International Conference on Intelligent Robots and Systems*, volume 2017-Septe, pages 2351–2358, 2017.

[35] Hamidreza Kasaei and Mohammadreza Kasaei. Throwing objects into a moving basket while avoiding obstacles. In *2023 IEEE International Conference on Robotics and Automation (ICRA)*, pages 3051–3057. IEEE, 2023.

[36] Daniele Bianchi, Maria Grazia Antonelli, Cecilia Laschi, Angelo Maria Sabatini, and Egidio Falotico. Softoss: Learning to throw objects with a soft robot. *IEEE Robotics & Automation Magazine*.

[37] Nagamanikandan Govindan, Bharadhwaj Ramachandran, Pasala Haasith Venkata Sai, and K. Madhava Krishna. A novel hybrid gripper capable of grasping and throwing manipulation. *IEEE/ASME Transactions on Mechatronics*, 28(6):3317–3328, 2023.

[38] N. Govindan and A. Thondiyath. Design and analysis of a multimodal grasper having shape conformity and within-hand manipulation with adjustable contact forces. *Journal of Mechanical Robotics*, 2019.

[39] Charles R Qi, Hao Su, Kaichun Mo, and Leonidas J Guibas. Pointnet: Deep learning on point sets for 3d classification and segmentation. In *2017 IEEE Conference on Computer Vision and Pattern Recognition (CVPR)*, pages 77–85. IEEE, 2017.